Ch 11
(285/1960)

UDC 669.018:669.3.721.782(084.2)

CHEMISTRY INCLUDING METALLURGY SERIES No. 11

L. J. ASCHAN

Studies on the ternary system Cu-Mg-Si

Finnish Contribution No. 16

HELSINKI 1960

ACTA POLYTECHNICA SCANDINAVICA

. . . a Scandinavian contribution to international engineering sciences

Published under the auspices of the Scandinavian Council for Applied Research

in *Denmark* by the Danish Academy of Technical Sciences

in *Finland* by the Finnish Academy of Technical Sciences, the Swedish Academy of Engineering Sciences in Finland, and the State Institute for Technical Research

in *Norway* by the Norwegian Academy of Technical Science and the Royal Norwegian Council for Scientific and Industrial Research

in *Sweden* by the Royal Swedish Academy of Engineering Sciences, the Swedish Natural Science Research Council, and the Swedish Technical Research Council

Acta Polytechnica Scandinavica consists of the following sub-series:

Chemistry including Metallurgy Series, Ch
Civil Engineering and Building Construction Series, Ci
Electrical Engineering Series, El
Mathematics and Computing Machinery Series, Ma
Mechanical Engineering Series, Me
Physics including Nucleonics Series, Ph

For subscription to the complete series or to one or more of the sub-series and for purchase of single copies, please write to

ACTA POLYTECHNICA SCANDINAVICA PUBLISHING OFFICE

Box 5073
Stockholm 5 Phone 61 47 53

This issue is published by
SWEDISH ACADEMY OF ENGINEERING SCIENCES IN FINLAND
Helsinki, Finland

ERRATA

Page 10, Table II for: MORRAL—WESTGREN
read: MORRAL—WESTGREN

32, line 5 for: liq. $\lesssim \delta + \eta$
read: liq. $\leftrightarrows \delta + \eta$

42, line 9 for: σ-phase
read: ϱ-phase

44, line 1 for: 550°
read: 552°

45, Table X, line 2
for: 830°
read: ~ 826°

53, line 6 for: 122 ..... **851**/(737)/716 sol. /618
read: **831**/ etc.

53, line 16 from bottom of page
for: 170 ..... 764/716/(633)
read: (663)

57, line 5 for: 241 ..... 891/815/765/(721)
read: /763/

59, line 14 for: 46 $\varkappa + \gamma$ 790°
read: $\varkappa + \gamma + (\delta)$ 790°

59, line 19 insert: 54 $\gamma + \varepsilon$ 770° $\gamma + \varepsilon$ 800°
the following line to read: 57 $\delta + \varkappa$ 805°

61, line 16 from bottom of page
for: 196 $\alpha + \eta + \sigma$
read: $\alpha + \gamma + \varrho$

61, line 8 from bottom of page
for: 207 $\sigma + \varepsilon + \sigma$
read: $\varrho + \varepsilon + \sigma$

63, last line for: 271 $\tau' + \lambda + \nu$
read: $\tau' + \lambda + \nu$

UDC 669.018:669.3.721.782(084.2)

STUDIES ON THE TERNARY SYSTEM Cu-Mg-Si

by

L. J. ASCHAN

ACTA POLYTECHNICA SCANDINAVICA

Chemistry including Metallurgy Series No. 11
(AP 285, 1960)

Helsinki 1960. Valtioneuvoston kirjapaino

PREFACE

The work for the present study was carried out mainly in the years 1952 to 1957 at the Laboratory for Physical Metallurgy of the Institute of Technology (Helsinki).

The theme for this study was originally suggested to the author in 1948 by Dr. H. Unckel, D. Eng., now of Finspång, Sweden.

I wish to express my gratitude to Professor H. M. Miekk-oja, Ph. D., for good advice and friendly criticism during the second stage of this work. I am also indebted to Professor P. Rautala, D. Sc. (now of Purdue University) for valuable advice, especially regarding the presentation of the phase diagram as a three-dimensional model.

My thanks are due to Mr. C. af Hällström and Mr. K. B. Nordman at Tampella Ltd. for granting me leave of absence for the purpose of this work.

The melting of the alloy samples was carried out at the Metallurgical Laboratory of the State Institute for Technical Research. For this I am indebted to Professor M. H. Tikkanen, D. Sc. and Dr. P. K. G. Asanti, D. Eng., and also for permission to use its equipment for the thermal analyses; further to Mr. D. Granfelt for supervising the melting operations. The six X-ray precision diffraction patterns (with the 8.5 cm camera) were made by Dr. L. Hyvärinen, D.Sc., to whom my thanks are due.

The alloy analyses were mostly made by my former assistants in the Laboratory Department of Tampella Ltd. In this connection it is a pleasure to acknowledge the competent analytical work of Miss R. Danielsson, M. Sc. (Malmberget, Sweden), who also made the checking analyses in Table V.

I am also greatly indebted to the Editors of »Fonderie» and »Metal Abstracts» (J. Inst. Metals), respectively, for sending me copies of important papers not available in Finnish libraries.

The text has been read and corrected by Mrs. Jean Margaret Perttunen, B. Sc., to whom my thanks are due.

The financial support awarded me by the City of Tampere (through its »Committee for grants for scientific research») and by the institution »Svenska Tekniska Vetenskapsakademien i Finland» (»The Swedish Academy of Engineering Sciences in Finland») is herewith gratefully acknowledged.

My former Student Corporation (TF) awarded me one of its scholarship grants, for which my thanks are due.

Tampella Ltd.

Tampere (Tammerfors) April 1960.

The Author.

Table of contents.

INTRODUCTION

The copper alloys commercially known as »silicon bronzes» are either straight Cu-Si alloys or contain small amounts of one or two additional components besides copper and silicon.

These were originally developed to meet the need for a high-strength copper alloy with good electrical conductivity, but nowadays the silicon bronzes are recommended especially on account of their good weldability, or, in some cases, to conserve tin during times of shortage.

SMITH, ARRHENIUS and WESTGREN, and ANDERSEN have been the main contributors to our knowledge of the Cu-Si phase diagram, which is well established except for some details of the crystal structures. The ternary system Cu-Mg-Si has not been investigated thoroughly, and the diagram is more complicated than most of the others connected with the binary system Cu-Si.

The author first became interested in the system Cu-Mg-Si in connection with the use of silicon bronzes to conserve tin in bronze bearings and other castings. The investigation of which this work was originally a part concerned the mechanical properties of the silicon bronzes. It also raised the question of why the alloys of the face-centred cubic Al with Mg and Si were commercially successful, while those of the face-centred cubic Cu with the same two components were only a slight improvement on the binary Cu-Si alloys, and this only with minute additions of Mg.

The explanation depends on the unfavourable atomic sizes of both Mg and Si for solid solution in Cu, and in part on the influence of the intermediate compounds in the system Cu-Si. The ternary diagram was considered to be of some theoretical interest, and the investigation was directed towards establishing the phase distribution (in the form of an isothermal section) and the equilibrium reactions, especially in the copper corner of the diagram.

1. Summary of earlier research

a) *The binary system Cu-Si.*

The phase diagram of the binary system Cu-Si (C. S. SMITH, Metals Handbook, 1948 edition), is reproduced here as fig. 1.

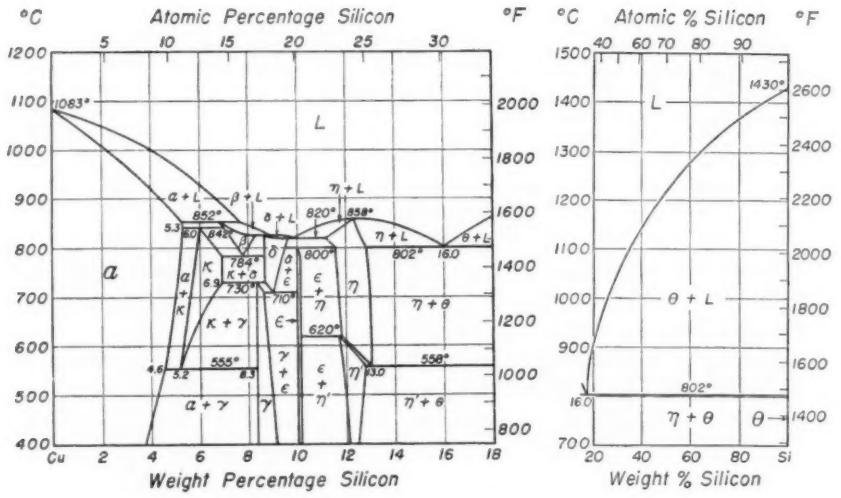

Fig. 1. The phase diagram Cu-Si (SMITH, ANDERSEN).
(ASM Metals Handbook, 1948 ed.)

The earlier work on this system has been discussed by HANSEN [1], and by SMITH [2, 3, 4]. The diagram in fig. 1 is well substantiated through the microscopical work of SMITH and the X-ray work of ARRHENIUS and WESTGREN [5], and ANDERSEN [6]. *)

A summary of the X-ray work on the various crystal structures is presented in Table I, and the corresponding lattice parameter values are given in Table II. These data have been discussed by PEARSON [7].

The data for the α-, γ- and ε-phase lattices seem well established. The $\varkappa$-phase was first observed by VOCE [8] in his study of the ternary silicon-manganese-copper alloys. Here, as well as in those of the binary Cu-Si system, it appears in unhomogenized cast specimens, forming rounded blocks in the microstructure. The reason why $\varkappa$ had not been detected earlier is that alloys containing $\alpha+\varkappa$ have a very peculiar striated structure, resembling heavily twinned α. This structure does not spheroidize on annealing, which, since it is difficult to distinguish from pure α, accounts for the earlier concepts of an α-area with a boundary sloping towards the β-region with nearly 7 % Si. The eutectoidal breakdown of $\varkappa$ into $\alpha+\gamma$ below 555° takes place with extreme sluggishness unless the alloys are cold-worked before annealing [4, 6].

*) NOWOTNY and BITTNER [43] reported that they could not confirm the existence of the ε-phase. This may be because they annealed the samples in lump form, as the δ-phase is then markedly metastable. When powder samples are annealed, is the ε-phase easily verifiable.

TABLE I

Phase lattices in the binary system Cu-Si

Phase	Arrhenius—Westgren [5] Morral—Westgren [15]	Sautner [9]	Isawa [10] Okamoto [16]	Schubert—Brandauer [14]
α	face-centred cubic (A 1)			
β	—	hexagonal	body-centred cubic (A 2)	$Cu_{84}Si_{16}$ b.c.c. 7.75 % Si (A 2)
$\varkappa$	hexagonal close-packed (called β)	hexagonal		$Cu_{87}Si_{13}$ (A 3 ε) *)
γ	β-manganese structure (A 13)			Cu_5Si β-Mn str. 8.11 % Si (A 13)
δ	deformed γ-brass type lattice	tetragonal	cubic $D8_2$	$Cu_{82}Si_{18}$ $D8_2$ (?) 8.82 % Si
ε	body-centred cubic ($D8_6$)	cubic, called η, 12.8 % Si		Cu_4Si $D8_6$ 9.93 % Si
η	hexagonal, similar to CsCl structure in β-brass superlattice			Cu_3Si 12.82 % Si D_2 rhombohedrally distorted (A 2 V) **)
η'	—	b.c. tetragonal (?), called ε; 12.26 % Si		
	— — —	— — —	— — —	— — —
θ	(= silicon) diamond structure (A 4)			

*) Schubert and Brandauer use this notation to cover those hexagonal structures where the axial ratio c/a decreases with increasing values of the valency electron concentration (Schubert : [13]).

**) This notation covers a type of rhombohedrally distorted b.c.c. structures, in which the axial ratio c/a is less than the theoretical value 1.225.

The data for the β-, δ- and η-phases are conflicting. Some of the results of Sautner [9] differ clearly from those of other research workers, especially in the ε-η-area. Among other authors who have contributed to the subject are Isawa [10] and Iokibe [11]. The latter claimed to have found evidence of a $\eta \leftrightarrows \eta' \leftrightarrows \eta''$ transformation.

The paper by Schubert and Brandauer [14] is mainly an examination of the binary system Cu-Ge in connection with the studies of Schubert [12, 13] on distorted hexagonal (A 3-) and body-centred cubic (A 2-) lattices in general. The apparent similarity of the Cu-Si and Cu-Ge phase diagrams is stressed, and Cu_3Si is said to be similar to (»isotyp mit«) Cu_3Ge. This latter phase has a rhombohedrally distorted A 2-type lattice (»trigonal verzerrt«).

TABLE II

Lattice parameters

Phase	Lattice parameter	Author
α	$a = 3.6077 + 0.00065 \times C$ kX (C = atomic % Si) $a_{max} = 3.6153$ kX	ANDERSEN [6]
$\varkappa$	$a_1 = 2.5539$ kX (10.9 atomic % = 5.13 wt. % Si) $c/a = 1.6353$ $a_1 = 2.5563$ kX (14.6 atomic % = 7.02 wt. % Si) $c/a = 1.6328$	ANDERSEN [6]
β	$a = 2.848$ kX (?)	ISAWA [10]
γ	$a = 6.210$ kX	ARRHENIUS—WESTGREN [5]
δ	$a = 8.48_9$ kX	ISAWA [10]
ε	$a = 9.694$ kX	MORRAL—WESTGREN [15]
η	—	
η'	$a = 9.21$ kX (?) $c/a = 1.15$	SAUTNER [9]
θ(=Si)	$a = 5.4282$ Å	

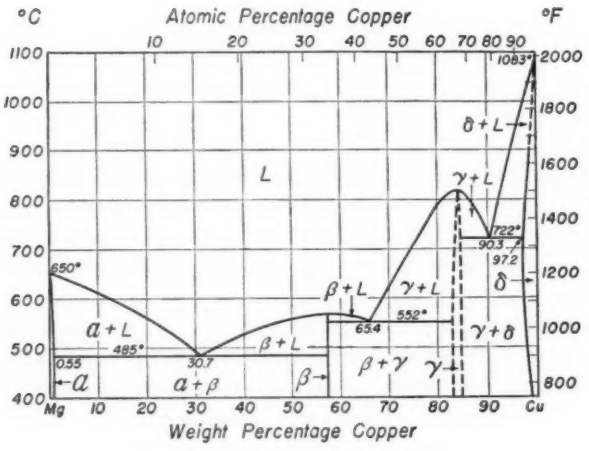

Fig. 2. The phase diagram Cu-Mg (JONES).
(ASM Metals Handbook, 1948 ed.)

b) *The binary system Cu-Mg*

The phase diagram of the binary system Cu-Mg (fig. 2) is mainly based on the work of JONES [17]. He investigated the liquidus and solidus lines, using vacuum-melted ingots, and also the microstructure of alloys with different Mg contents. The existence of the two intermediate phases Cu_2Mg (γ) and $CuMg_2$ (β) had already been established by SAHMEN in 1908. FRIAUF [18] determined the crystal lattice of the Cu_2Mg phase, and found it to be face-centred cubic, with a lattice parameter of 6.99 kX. $CuMg_2$ has an orthorhombic structure [19, 20, 21].

SEDERMAN [22] was able to verify the existence of a solubility range for Cu_2Mg by means of X-ray diffraction studies. The lattice parameters found by him are different on the two sides of the composition Cu_2Mg (Table III).

TABLE III

Lattice parameter values for Cu_2Mg, according to SEDERMAN [22]. Interpolation to 450° (present author).

Temperature	Lattice parameter, kX	
	$\alpha + \varrho$ region (fig. 10)	$\varrho + \nu$ region (fig. 40)
600°	7.0087	—
500°	7.0133	7.0518
400°	7.0185	—
380°	—	7.0343
450°	7.0159 (interpolated)	

7.016 kX = 7.030 Å

The solubility of Mg in Cu is 2.8 % at 722°C, diminishing to about 1.2 % at 400°.

The Cu_2Mg structure is one of the three main »Laves phase» types, of the general composition MgX_2. *) These were first studied by LAVES and WITTE [24] in some ternary alloys with magnesium. The structures change along the section MgX_2—MgY_2 in the ternary system (Mg—X—Y), and are dependent on the electron concentration. The cubic $MgCu_2$ type is stable only at low e.c. values. Cf. also [23].

c) *The binary system Mg-Si*

The phase diagram of the binary system Mg-Si is based on the work of VOGEL [25], and WÖHLER and SCHLIEPHAKE [26]. This constitutes a

*) The others are $MgZn_2$ (hexagonal) and $MgNi_2$ (hexagonal, with different stacking of the component planes). $MgNi_2$ is an intermediate structure between those of $MgCu_2$ and of $MgZn_2$.

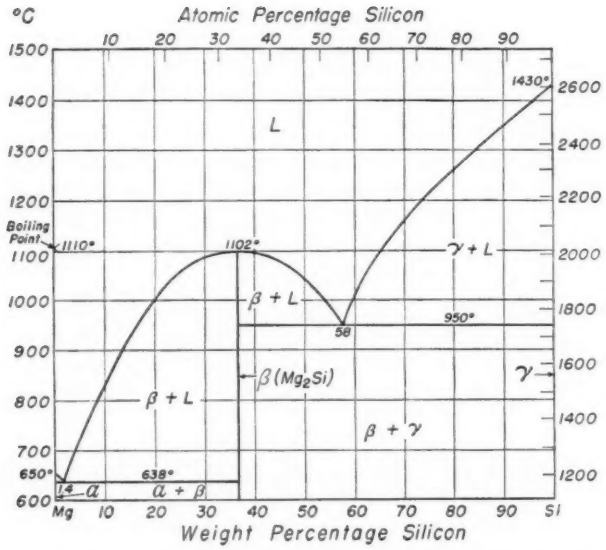

Fig. 3. The phase diagram Mg-Si (KLEMM and WESTLINNING). *(ASM Metals Handbook, 1948 ed.)*

system with an intermediate compound, Mg_2Si (β), and no solid solubility (fig. 3).

OWEN and PRESTON [27] determined the lattice parameter of Mg_2Si, and obtained a = 6.391 kX. They proposed that the structure is face-centred cubic, CaF_2 type. KLEMM and WESTLINNING subsequently corrected the lattice parameter value to 6.338 ± 0.002 Å [28].

d) *The ternary system Cu-Mg-Si*

The ternary system Cu-Mg-Si has been investigated by PORTEVIN and BONNOT [29], and WITTE [30, 31, 32].

PORTEVIN and BONNOT employed the »Klärkreutz» method for determining pseudo-binary sections in ternary diagrams (fig. 4). The solid solubilities in this system are said to be faint or non-existent (»faible ou nulle»).

They found a ternary compound Cu_3Mg_2Si with the melting point 927° C. The vertical sections drawn from the point corresponding to the composition Cu_3Mg_2Si to $CuMg_2$ and Mg_2Si were found to be pseudo-binary. The authors investigated the area Mg—$CuMg_2$—Cu_3Mg_2Si—Mg_2Si, and found two invariant four-phase equilibria: a ternary transition (2:2) reaction (π) at 508° and 38 % Cu, 0.6 % Si:

$$Cu_3Mg_2Si + \text{liq.} \leftrightarrows CuMg_2 + Mg_2Si,$$

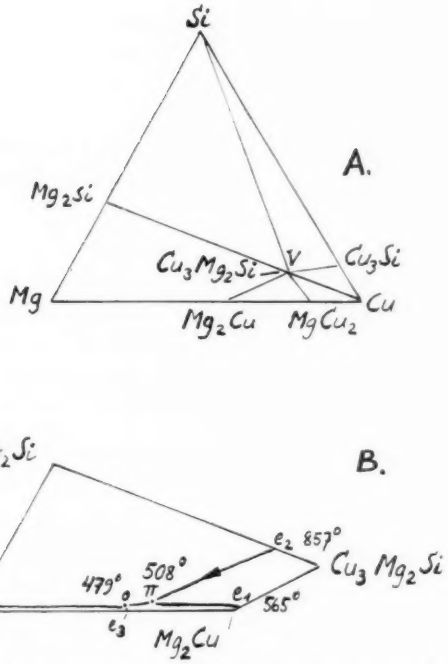

Fig. 4. A) the ternary diagram Cu-Mg-Si, showing pseudo-binary sections and the compound Cu_3Mg_2Si; B) solidification of alloys in the Mg-rich corner (PORTEVIN and BONNOT).

and a ternary eutectic (*o*) at 479°, and 32.5 % Cu, 0.4 % Si:

$$\text{liq.} \rightleftarrows Mg + CuMg_2 + Mg_2Si.$$

The copper corner of the diagram was not investigated.

WITTE made an X-ray study of the Cu-Mg-Si alloys on the section between the composition $MgCu_2$ and »$MgSi_2$» (calculated), in the course of an investigation on »Laves phases» of the MgX_2 type. The liquidus point determinations are presented in the form of a vertical section along the line mentioned above, with 33.3 atomic per cent of Mg (fig. 5).

The results of WITTE may be summarized as follows:

— Si is soluble in the $MgCu_2$ phase up to an amount which in WITTE's notation reads »19 molecular per cent of $MgSi_2$», i.e. 7.75 weight per cent Si,

— when this concentration is exceeded, there appears a $MgNi_2$ type phase, stable at higher temperatures (over 870°), and corresponding to the composition »25 molecular per cent $MgSi_2$», i.e. 10.75 % Si,

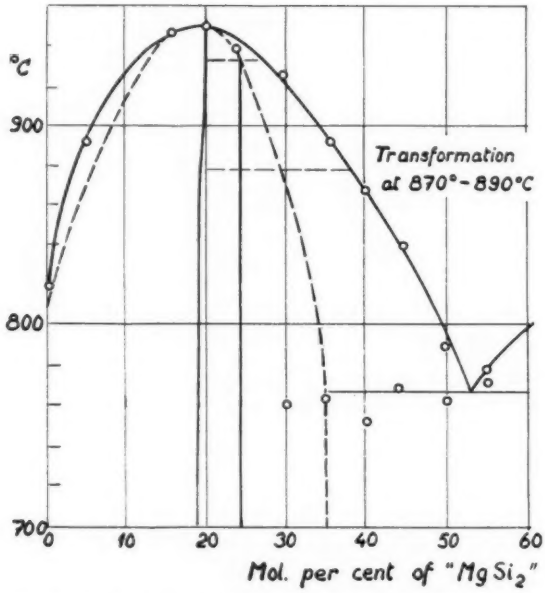

Fig. 5. Part of the vertical section $MgCu_2$—»$MgSi_2$«, showing incomplete mutual solubility of the Laves phases (type MgX_2), and the transformation at about 870° C (WITTE).

— with the same alloy composition but at lower temperatures (below 870°), there exists a phase of a new Cu_3Mg_2Si type. Its structure was determined by WITTE by means of X-rays. It resembles the previously known hexagonal Laves phase $MgZn_2$. The structure is ordered, in that the Si atoms occupy the positions: 000, 00½, and the Cu-atoms all the other positions ascribed to Zn atoms in $MgZn_2$. The lattice parameter values found were a = 5.00, c = 7.87 kX, c/a = 1.57,

— a hitherto unknown ternary compound was found at approximately 14.5 % Si, 11 % Mg. X-ray powder patterns showed a complex face-centred cubic lattice, a = 11.67 kX. The number of atoms was calculated from this value and from the density, which was found to be 5.63. The results correspond to the composition $Cu_{16}Mg_6Si_7$, and 116 atoms in the unit cell *),

— the stability range of this compound was found to be very restricted, and deviations of the magnitude of 0.5 % (stoichiometric) cause precipitation of other phases. The sample which had the maximum

*) A later paper by NAGORSEN and WITTE [32] gave the lattice parameter value a = 11.65 ± 0.02 Å (alloy with 14.21 % Si, 10.36 % Mg). Cf. also fig. 34.

amount of the ternary phase had a composition deviating from the theoretical $Cu_{16}Mg_6Si_7$, but WITTE supposed that Mg losses during melting were the cause of this difference.

A list of all the known phases in the ternary system Cu-Mg-Si with the Greek letter symbols used in the present work is included in Table IV. The lettering sequence is arranged in the order: Cu—Si—Mg—ternary compounds.

TABLE IV.

Symbols used for existing phases in the ternary system Cu-Mg-Si

The binary system Cu-Si:	
Solid solution of Si in Cu (fig. 1)	α
Intermediate phase	β
Intermediate phase	$\varkappa$
Intermediate phase »Cu_5Si»	γ
Intermediate phase	δ
Intermediate phase	ε
Intermediate phase »Cu_3Si» at higher temperatures	η
Intermediate phase »Cu_3Si» at lower temperatures	η'
Silicon	θ
The binary system Si-Mg:	
Intermediate phase Mg_2Si(β, fig. 3)	λ
The binary system Mg-Cu:	
Solid solution of Cu in Mg (α, fig. 2)	μ
Intermediate phase $CuMg_2$ (β, fig. 2)	ν
Intermediate phase Cu_2Mg (γ, fig. 2)	ϱ
Ternary compounds:	
$Cu_{16}Mg_6Si_7$	σ
Cu_3Mg_2Si, high-temperature phase	τ
Cu_3Mg_2Si, low-temperature phase	τ'
	16

2. Scope of the present work

It appears from the preceding literature survey that a large part of the ternary Cu-Mg-Si diagram, especially the region near the copper corner, is still virtually unknown.

The scope of the present work is:

to draw a part of the isothermal section at 450° (comprising the copper corner of the ternary diagram),

to describe the corresponding part of the liquidus surface,

to determine the reactions of the four-phase equilibria, especially those with the liquid phase present,

to check the various lattice parameter values reported in the literature.

I. EXPERIMENTAL METHODS AND PROCEDURE

For the purposes of the present work, 250 ternary alloys were prepared and analyzed. Powder samples of the various alloys were heat-treated at 450°. The phases present were identified from the corresponding X-ray powder diffraction photographs. The results were utilized in drawing the isothermal section.

Thermal analysis was used for determining the temperature levels of the four-phase equilibria, and the liquidus point values utilized in depicting the liquidus surface.

Some additional X-ray work was carried out for checking a number of lattice parameter values.

1. Materials

The materials used for preparation of the alloy samples were as follows:

Copper: Standard OFHC copper, cast into wire bars, supplied by the Outokumpu Co. Ltd. The copper content was given by the manufacturers as 99.98 % plus.

Silicon: Commercial 97—98 % silicon of unknown origin was used. It was supplied by Messrs. C. M. Truedson, of Stockholm, Sweden. This brand contained some carbide and phosphide, and a substantial amount of iron as oxide and silicate. After the purity of the first few alloys had been determined, the Tucker method [33] for chemical purification was applied. The soluble matter is dissolved in hydrochloric acid, and the residue is then heated with hydrofluoric acid in a platinum dish to remove any silica or silicates present. Then follows another treatment with HCl to dissolve the iron oxide originating from the silicates.

The author is indebted to Mr. L. LUND, formerly of the Department of Analytical Chemistry, The Institute of Technology (Helsinki), for a spectrometer analysis of a sample of the purified silicon. This gave the following approximate ranges for impurities:

Fe	about	0.1 %	Al	about	0.1 %
Mn	»	0.1	Ti	»	0.001
Ca	»	0.1	Cr	»	0.001

Thus the Si content of the treated material is about 99.5 % or more.

Magnesium: As the pure metal was not available, the silicon-magnesium alloy »CMSi», with a nominal composition of 1.5 % Si (range 0.5 to 2 %), Fe 0.1 %, Mg bal., was used instead.

This was originally added to molten copper to give a »hardener» alloy with 15 or 50 % Mg, but was subsequently added to the melts as such.

2. Melting and casting

The alloys were prepared in the metallurgical laboratory of the State Institute for Technical Research, in the 30 kW, 3 800 cycle ASEA high-frequency furnace. The crucibles for melting were made from graphite electrodes, supplied by Messrs. Lokomo Ltd.

A sodium fluoride flux is recommended by SMITH [2] for use with silicon bronzes. It was found that impure NaF contained some Al, and contamination was subsequently avoided by using flux of analytical reagent purity only.

The method for alloying consists in melting down the copper lumps, then adding the finely ground silicon powder mixed with 5 to 10 % NaF while stirring the melt with an alumina rod, and lastly adding the magnesium alloy in lumps. The addition of the first 10 grams of Mg cools the melt, and the losses by evaporation on adding more Mg are insignificant in comparison. The silicon powder must be added in amounts about 10 % in excess, and the yield is still lower when the Si content nears or exceeds 12.5 % (the η-phase composition in Cu-Si alloys).

The pouring temperatures ranged from 1 000° to 1 180°. The melting time per charge varied between 10 and 25 minutes. The alloy samples were poured into tapered chill moulds, in which 800 g test bars of copper-rich alloy could be cast. For the alloys richer in Si and Mg, the amount melted was 450 g. The moulds were covered with a soot layer from an acetylene flame, to facilitate the removal of the ingots.

From the lower part of the ingot specimens were taken for the chemical analysis and for the microscopical work and filings for X-ray examination. The remaining part was used for thermal analysis.

3. Chemical analysis

All alloy samples were analyzed to determine the Si and Mg contents. Iron, the principal impurity, was also determined in connection with the Mg-phosphate precipitation. Copper was determined for checking purposes only.

The silicon content in the alloys was determined by the following method:

1 g of the crushed alloy is dissolved in 25 ml nitric acid (1.19). 10 ml hydrochloric acid is added and the solution evaporated. The residue is heated to decompose the nitrates, then redissolved in hydrochloric acid, the solution evaporated and the residue heated 1h at 130° C. 10 ml hydrochloric acid (1.12) is added. The solution is heated, diluted and filtered. The filtrate is evaporated to dryness and heated at 130° C, and the above-mentioned cycle is repeated once more. The residue from the filtrate is filtered off through another paper. Both the precipitates are dried, ignited, and weighed together as SiO_2. The iron content is precipitated, as the hydroxide, with ammonia.

When the copper content is to be determined, the filtrate is evaporated with a small amount of sulphuric acid and diluted with water, and the copper precipitated cathodically on a platinum electrode.

For the determination of the magnesium content, 0.5 g tartaric acid and 2 to 3 g ammonium chloride are added to the filtrate. Then 1 ml of a 2 M solution of diammonium phosphate is added for every 10 mg of MgO in the sample (calculated from the nominal alloy composition). Methyl red is added as indicator. The precipitation is inoculated with a drop of a diluted slurry of Mg-phosphate in water whilst concentrated ammonia is added until the indicator changes colour, plus 13 ml then added in excess. The solution is stirred during and after the precipitation. The precipitate is filtered, washed with 2.5 per cent ammonia solution, dissolved and precipitated once more to eliminate any traces of copper still present. The final filtered precipitate is ignited and weighed and the Mg content calculated from the amount of pyrophosphate ($Mg_2P_2O_7$) obtained [34].

In the cases where the alloys were analyzed for both copper and the alloying elements, the sum of the analytical percentages lay between 99.93 and 100.02 per cent (Table V). The weighing errors predominantly affect the accuracy of the copper determinations (cf. SMITH, [4], p. 316).

TABLE V.

Test analyses for checking purposes

Alloy No	Si %	Mg %	Fe %	Cu %	Σ %
89	2.49	1.85	0.10	95.51	99.95
123	11.50	1.92	0.08	86.50	100.0
131	4.47	2.06	0.07	93.33	99.93
151	9.74	2.06	0.09	88.09	99.98
176	1.97	4.86	0.09	93.06	99.98
181	10.20	4.84	0.09	84.83	99.96
187	13.31	5.99	0.22	80.47	99.99
189	12.63	5.26	0.19	81.90	99.98
198	10.70	7.07	0.30	81.86	99.93
267	11.32	27.90	0.59	60.13	99.94

4. Heat treatment

The cast ingots were subjected to a soaking type heat treatment. This was carried out in an electric annealing furnace at the State Institute for Technical Research. The standard treatment was 168^h at 450° ± 5° C.

Additional annealing of samples for checking purposes (specimens for microscopical examination) was carried out for 2^h to 800^h at varying temperatures up to 700° C, followed by a water quench. At still higher temperatures, up to 830° C, the alloy samples were heat-treated after being sealed into glass tubes. For some alloys containing the slowly decomposing kappa phase the annealing time was 810^h at 550° C.

In an attempt to retain the high-temperature β- or δ-phases, respectively, several alloy samples were sealed in tubes of Pyrex glass, annealed at 770°—830°, and quenched in liquid air or with solid carbon dioxide.

The equilibrium heat treatment of the powder specimens for X-ray diffraction studies was carried out in evacuated Pyrex glass tubes in a laboratory furnace with L-N Micromax controller (± 2° C).

5. Microscopical examination

Heat-treated alloy specimens were examined with the microscope to determine the alloy constituents after annealing, and to compare the microstructures with those of the alloys as cast.

The specimens for microscopical work were ground and polished on emery paper to 6/0 fineness. The final polishing was carried out on No. 900 flannel cloth on a rotating disk with Dujardin's alumina suspension No. 3. Most of the hard samples were by then ready for microscopical examination, but in some cases additional hand polishing on Selvyt cloth was required.

It was difficult in some cases, notably with specimens containing the η- or τ-constituents, to obtain pit-free surfaces. The kappa alloys often developed corrosion pinholes during the final polishing stages. The brittle alloys were susceptible to scratching by particles dislodged from the sample edges.

The following etching reagents were used:

(a) Acid ferric chloride:

Ferric chloride	5 g
Hydrochloric acid	30 ml
Water	100 »

(b) WOLFE'S citric acid electrolytic etchant [35]:

Citric acid	100 g
Hydrochloric acid	3 ml

Ethyl alcohol	20	ml
Water to	1 000	»

(c) Modified ammonia—hydrogen peroxide reagent [4]:

Hydrogen peroxide, 30 %	20	parts
Water	5	»
Potassium hydroxide, 20 % solution	5	»
Ammonia, sp. gr. 0.90	50	»

Reagent (a) was found suitable for most of the alloys studied, but (b) gave a better colour contrast in some cases.

Reagent (b) was used for anodic etching at 10 volts for 2 to 3 secs., and gave a grey, filmy precipitate on the surface of the specimen. It could be removed either by swabbing, or by a short immersion in acid ferric chloride. The double treatment, with (b) followed by (a), gave good results on alloys containing the σ-phase.

Reagent (c) was proposed by SMITH [4] for identifying the kappa-phase. In the copper-rich alloys containing α, $\varkappa$ and γ it outlines the γ-phase and reveals coring in the dendrites. The ternary eutectic in these alloys, on the other hand, shows up more distinctly when etched with reagent (a).

A Reichert MeF metallograph was used for the microscopical work. In general, Kodak O 800 orthochromatic plates were used. Most of the intermediate phases were photographed with oblique illumination, to bring out the relief effect, which depends on the difference in hardness of the various constituents. For micrographs in colour, a Kine-Exakta camera for 35 mm film was used. For this purpose, the lens was removed, and the image was focussed with the aid of the viewing mirror. The film used was Kodachrome A, for artificial light. The exposure time ranged from 5 to 15 seconds at magnifications from 20 to 550 diameters.

6. X-ray powder samples and equipment

For the purpose of determining the alloy composition at 450°, and investigating the four-phase reactions, the heat-treated and quenched powder samples were studied by means of X-rays. The phases present were identified from their characteristic reflection patterns.

The powder samples for X-ray analysis were as a rule taken from the already heat-treated microscopical specimens (450°) by filing. The δ-phase alloys used for the lattice parameter determination formed an exception, as the chill-cast samples gave less ε-contamination in the powders. The filings were screened through a sieve with 0.06 mm aperture and collected in Pyrex glass tubes. These were evacuated with a vacuum pump, sealed off, and heat-treated anew. The temperatures used were generally the

following (Appendix B): 450°; 600°—620° (kappa-alloys); 710°—790° at 20° intervals, and 800°—830° at 5° intervals.

Magnesium has an appreciable vapour pressure at higher temperatures.*) There was often a black to brownish film of condensed metal on the inside surface of the tube after the heat treatment. This was noticeable when samples containing phases with high Mg contents, such as ϱ, σ and especially ν, were heat-treated. Errors in the phase identification method are not serious, however, except at the $\alpha/\alpha + \varrho$-phase boundary, where the significant ϱ-reflections may be weakened.

To determine the order of magnitude of the error by vaporization, a powder sample of alloy 137 (6.1 % Si, 2.49 % Mg) was heat-treated, and quenched in water from 750°. The sample was analyzed polarographically at the Chemical Institute of Åbo Akademi. The Mg content had diminished from 2.49 % to 2.2 % Mg.

The powder diagrams for phase identification were determined by the author in the Laboratory for Physical Metallurgy at the Institute of Technology (Helsinki) with a powder camera with 5.74 cm diam. The exposures were on Gevaert or Ilford Industrial X-ray film, without screens.

A focussing camera of radius 4.96 cm was used by the author for some lattice parameter determinations in the Laboratory for Technical Physics. The δ- and η-phase powder reflection patterns were studied by means of a precision camera of 8.5 cm diam., with the STRAUMANIS film arrangement. The lattice parameter values for the ϱ-phase were also checked with this camera.

7. Accuracy of the lattice parameter determinations

The results of the lattice parameter determinations were as far as possible calculated according to the extrapolation method of COHEN **). The errors (other than film shrinkage) are stated by COHEN to be approximately proportional to the function $\sin^2 2\theta$ for angles of $\theta > 70°$. The method is equivalent to an error calculation of »least squares».

The BRADLEY film arrangement was used with the 5.74 cm camera. The readings of the θ-angles were corrected from the reference marks from a slit across the film gap. For the σ-phase lattice parameter, the COHEN calculation gives an average error of $\pm$ 0.011 Å.

*) The »Landolt-Börnstein Tables» give the values of 9 mm Hg at 623° and 20 mm at 748° C.

**) COHEN [36, 37]; BUERGER [38]. For cubic crystals, the functions α ($= h^2 + k^2 + l^2$), $\sin^2\theta_{hkl}$ and δ ($= \sin^2 2\theta_{hkl} \times 10^3$) were tabulated for the high-order reflections used. The values of $\Sigma\alpha^2$, $\Sigma\alpha\delta$, $\Sigma\delta^2$, $\Sigma\alpha \sin^2\theta$ and $\Sigma\delta\sin^2\theta$ were computed. The equations are:

$$\Sigma\, \alpha^2\ \mathrm{A} + \Sigma\, \alpha\delta\ \mathrm{D} = \Sigma\, \alpha\ \sin^2\theta$$
$$\Sigma\, \alpha\delta\ \mathrm{A} + \Sigma\, \delta^2\ \mathrm{D} = \Sigma\, \delta\ \sin^2\theta$$

From the value of A, the lattice parameter $a = \dfrac{\lambda}{2\sqrt{A}}$ was calculated.

With the 8.5 cm precision camera, the accuracy of the results was affected, inter alia, by the fineness of the powder sample. In the most reliable determination of the ϱ-phase lattice parameter the error averaged $\pm$ 0.003 Å, but with diffuse high-order reflections this increased to $\pm$ 0.01 Å.

The COHEN method could not be used with the asymmetrical focussing camera. Graphical extrapolation to $\sin^2 \theta = 1$ gave errors of the magnitude $\pm$ 0.01 Å.

8. Equipment for thermal analysis

The melting point determinations were carried out according to two methods: the direct reading method, one thermocouple only, and the differential reading method, with two thermocouples, and a second crucible containing a reference metal, e.g. Ag.

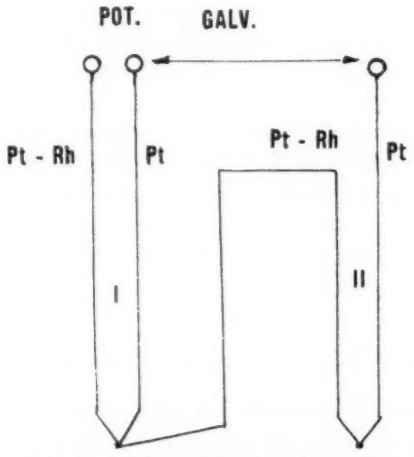

Fig. 6. Set-up for differential thermal analysis (KEHL).

The set-up for taking differential readings during thermal analysis is described by KEHL [39]. A Pt/Pt, 10 % Rh thermocouple was used, with a precision »Doran» potentiometer. The positive lead of the second thermocouple was welded to the joint of the first, and its joint was immersed in a reference crucible containing pure silver (fig. 6). The potentiometer was guaranteed exact within 0.001 mV, and checked with readings on pure silver. A sensitive »Radiometer» type GVM 21 galvanometer was used for recording the temperature differences between the thermocouple in the molten alloy and the reference thermocouple, the readings being taken on the 0.01 mV scale. The rate of cooling could be controlled by varying the furnace current. The time was recorded at 2° intervals (fig. 7).

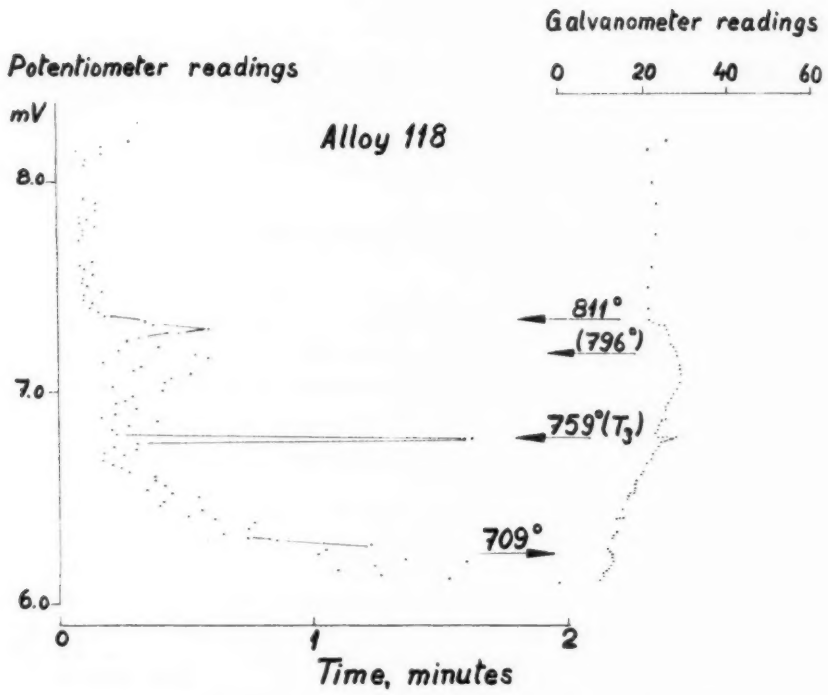

Fig. 7. Thermal analysis with the differential galvanometer method. Alloy 118.

Most of the readings on alloys with more than 5 % Mg were plotted as direct type curves, the potentiometer only being used, and readings taken every 10th second (fig. 8).

The alloys to be studied were melted in a Pythagoras crucible of 20 mm diam. in a resistance furnace. The furnace current was controlled by means of a rheostat. About 30 g of the copper-rich alloys were used for a cooling curve determination. After the cooling curve readings had been taken, the sample was remelted and poured out from the crucible. The melt was protected against excessive evaporation of Mg in the crucible by an oxide film on the surface.

Most of the Mg losses occur whilst the sample is being poured into an open mould, after being remelted, when some burning is apparent. In some cases, a part of the melt adhered to the crucible. A number of analyses were made on the remelted samples, either poured or from the crucible »skull», and the results were compared with the original alloy composition (Table VI).

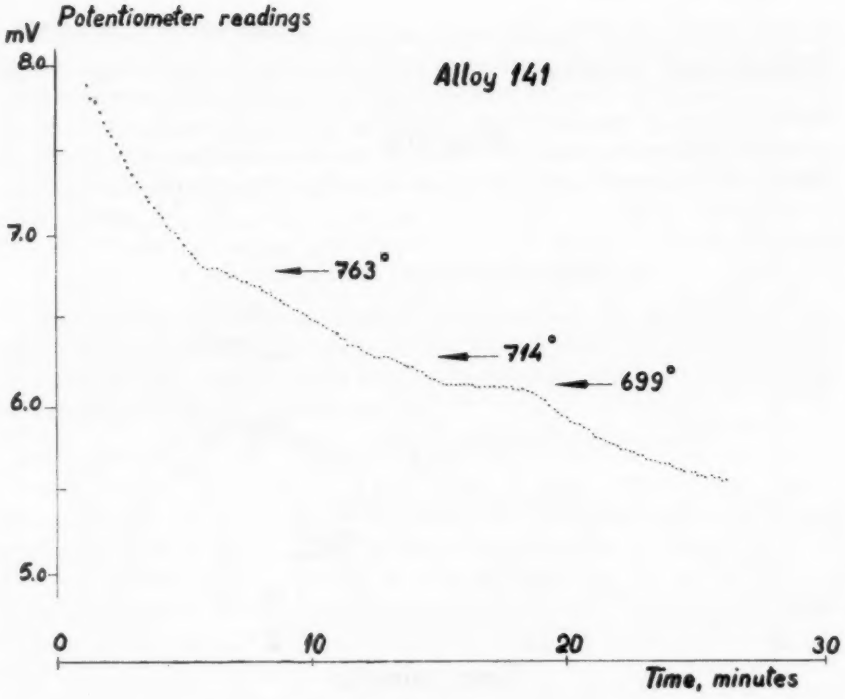

Fig. 8. Thermal analysis with potentiometer only. Alloy 141.

TABLE VI.

Check analyses on alloy samples after thermal analysis

Alloy	As cast		Remelted after thermal analysis and recast	
	% Si	% Mg	Si %	Mg %
36	6.10	0.79	5.87	0.27
42	7.60	0.61	7.59	0.36
61	9.10	0.43	9.10	0.35
115	9.75	1.16	9.7	0.58
			Solidified in crucible after thermal analysis	
			% Si	% Mg
74	9.8	0.93	10.5	0.74
82	7.98	0.72	7.95	0.70
166	9.10	3.07	9.11	2.28

II EXPERIMENTAL RESULTS

The alloy powder samples were studied by means of X-rays for the the purpose of obtaining the phase distribution at various temperature levels (cf. Appendix B). These results, together with the thermal analyses, form the basis for the evaluation of the four-phase equilibria.

1. Space lattices of phases in the binary and ternary systems

A comparative drawing of the X-ray powder diffraction patterns used for phase determinations is included as *Appendix C*. This is based mainly on work with the 5.74 cm camera.

A special survey was made of the five phases β, δ, η, ϱ and σ. This also included some lattice parameter determinations. The results are summarized below.

a) *The β-phase*

Samples of alloy 45 (8.2 % Si, no Mg) were annealed at 830° C and quenched in liquid air. No diffraction lines from β were visible. A powder sample of alloy 41, containing 7.7 % Si, 0.15 % Mg, was quenched in water from 820° C, but again no diffraction lines from β could be observed (cf. Appendix B).

b) *The δ-phase and the η-phase*

Powder samples of alloy 64 (9.21 % Si, no Mg) were quenched from 815° C. The δ-diffraction lines obtained from these (with the precision camera) agreed somewhat better with a f.c.c. lattice having a parameter »a» of about 12 Å*), rather than the previously found value 8.489 kX, b.c.c. [10].

No especial splitting-up of the δ-phase diffraction lines [5] could be observed from the X-ray films.

Powder samples of alloy 80 (12.5 % Si, 0.18 % Mg) were studied by means of X-rays for the purpose of obtaining the η-phase diffraction lines.

*) $a = 11.999 \pm 0.008$ Å, as obtained by the COHEN method [40]. This value would conform with a unit cell with 144 atoms (118 Cu, 26 Si), of a type not previously known. Cf. also [43]: B 2 (CsCl type).

These agree roughly with a cubic lattice in which a = 10.95 Å. The strong doublet at θ = 22.5 degrees (Appendix C) and some other reflections, however, suggest a Cu_3Ge type, rhombohedrally distorted cubic lattice [14], which in this case can be represented by a hexagonal one, with a = 10.22 Å, c = 12.30 Å, and c/a = 1.20 [40].

The results of SAUTNER [9] are not supported by the present work.

No differences were observed in the X-ray diffraction patterns between cast or quenched samples (with η), and samples annealed below 620° (η'). Cf. ref. [5].

c) *The ϱ-phase*

It has been shown by WITTE [30, 31] that there is considerable solid solubility for Si in the ϱ-phase. The lattice parameter shows a marked decrease with higher Si contents.

Two series of ternary alloys, with 8 % Mg and 16 % Mg, respectively, were prepared for the determination of the lattice parameter changes. For the alloys 201, 219, 249 and 259, the precision camera was used, and for the other samples (alloys 199 to 205 and 253 to 255, 258), the focussing camera. The results are given in Table VII and in fig. 9.

TABLE VII

Lattice parameter values for the ϱ-phase

(Powder samples, quenched from 450°)

Alloy	Si %	Mg %	Phase field	Lattice parameter Å	Precision camera Focussing camera
201	4.54	7.57	$\alpha + \varrho$	$6.980_0 \pm 0.004$	P
259	7.02	16.20	ϱ	$6.978_1 \pm 0.003$	P
219	5.97	10.3	$\alpha + \gamma + \varrho$	$6.968_6 \pm 0.009$	P
249	8.58	14.5	$\varrho + \sigma + \varepsilon$	$6.99_3 \pm 0.01$	P
203	0.15	8.9	$\alpha + \varrho$	$7.02_4 \pm 0.01$	F
204	0.77	8.08	$\alpha + \varrho$	7.02_2	F
199	1.77	7.89	$\alpha + \varrho$	7.01_1	F
205	2.79	8.01	$\alpha + \varrho$	7.00_4	F
200	3.59	7.86	$\alpha + \varrho$	6.99_1	F
253	0.25	15.5	$\alpha + \varrho$	7.03_0	F
254	1.58	15.6	$\alpha + \varrho$	7.02_9	F
251	2.86	15.7	$\alpha + \varrho$	7.01_5	F
258	3.14	16.5	$\alpha + \varrho$	7.00_5	F
256	4.35	15.97	$\alpha + \varrho$	7.00_6	F
252	5.4	15.9	$\alpha + \varrho$	6.99_4	F
255	6.26	15.8	$\alpha + \varrho$	6.98_5	F
259	7.02	16.2	ϱ	6.98_3	F

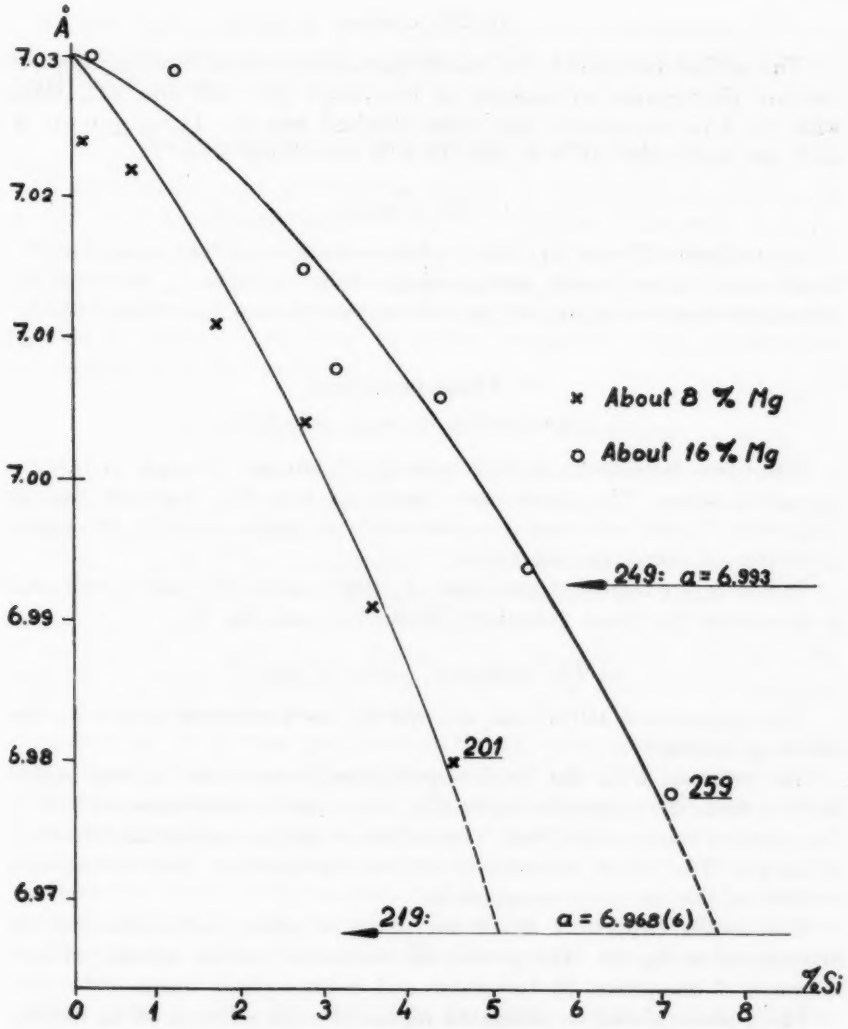

Fig. 9. Lattice parameter values for alloys containing ϱ.

The minimum lattice parameter value found for the ϱ-phase in equilibrium with α and γ is 6.969 Å (alloy 219)*). The lines in fig. 9 are assumed to curve slightly near the phase boundary (cf. ref. [7], p. 11).

*) From the values of SEDERMAN [22], a lattice parameter value of a = 7.030 Å is found by interpolation for the binary compound Cu_2Mg at 450° C (Table III).

d) *The σ-phase*

The author calculated the lattice parameter values from powder diffraction photographs of samples of the alloys 207, 223 and 247, taken with the 5.74 cm camera. The value obtained was $a = 11.70_6 \pm 0.011$ Å, with the high order (12 8 4) and (11 9 5) diffraction lines.*)

e) *The τ'-phase*

According to WITTE [31], the τ'-phase is hexagonal. The present author found that it is not easily distinguishable from the cubic ϱ- and σ-phases, because of some overlapping of characteristic diffraction lines (Appendix C).

2. Phase boundaries

a) *Determination of phase boundaries*

The phase boundaries at 450° were drawn on the principle of the disappearing phase. The phases were identified from the standard diagram (Appendix C), and were also compared with the phases found in the microstructures of corresponding alloys.

In the $\alpha + \varrho$-field, extrapolation of lattice parameter values was used to determine the phase boundary (Table VII and fig. 9).

b) *The isothermal section at 450° C*

The temperature 450° C was selected for the isothermal section for the following reasons:

The reaction with the lowest equilibrium temperature in the binary Cu-Si system, the kappa-decomposition into α and γ, takes place at 555° C. The selected temperature, 450°, thus allows a margin against undercooling of kappa. The phase composition at this temperature also corresponds roughly to that at room temperature.

The results (Appendix B) of the phase boundary determinations are summarized in fig. 10. The part of the isothermal section considered here comprises 7 one-phase, 10 two-phase and 6 three-phase fields.

The ϱ-phase shows an elongated region of solid solution (Si in Cu_2Mg, ref. [30, 31]; cf. II: 1c). The saturation limit is at about 8.3 % Si. For alloys in equilibrium with the α-phase, as 219, the limit for the Si content lies at about 7.8 %.

The results further confirm that the τ- and σ-phases have only very slight solubility ranges. But the γ- and ε-phases have appreciable ranges of solid solubility with Mg contents of about 2 per cent.

*) WITTE obtained $a = 11.67 \pm 0.011$ kX [30, 31], which corresponds to 11.69 Å. A later determination by NAGORSEN and WITTE [32] gave the value 11.65 ± 0.02 Å.

Of the high-temperature phases, β, $\varkappa$ and δ have disappeared entirely, η has been transformed into the η'-phase, and τ exists as the ordered hexagonal Laves phase τ' [30, 31]

3. The liquidus surface and the ternary reactions

A representation of the liquidus surface is obtained from the results of the thermal analyses (Appendix A), the principle being used that the starting points for the lines of twofold saturation in the ternary system are the peritectic or eutectic points in the binary phase diagrams. Some of the alloy microstructures are also useful for this purpose, since it is usually possible to identify from these the alloy constituent which is primarily crystallizing from the melt.

a) *The liquidus surface: general configuration*

Fig. 11 shows a basal projection of the lines of twofold saturation in the area from 0 to 16 % Si and 0 to 16 % Mg, with some isothermal contour lines of the liquidus surface.

Figs. 12 and 13 are photographs of three-dimensional models of two parts of the diagram. The α-, ϱ- and η-phase maxima are visible in fig. 12. In fig. 13, the lines of twofold saturation are shown with some of the planes of the four-phase equilibria, in the area 6 to 13 % Si, 0 to 4 % Mg. The surfaces of primary solidification are omitted in fig. 12, and only indicated with the corresponding phase symbol in fig. 13.

A part (A) of the basal projection in fig. 11, covering the primary solidifying regions of the phases from β to ε, or from 5 to 12 % Si, 0 to 5 % Mg, is shown in greater detail in fig. 14. Fig. 15 is a further magnified drawing of the area from 8 to 10 % Si, and 0 to 2 % Mg (B).

The following phases form surfaces of primary crystallization (fig. 11) in the copper corner of the diagram: α, β, δ, η, $\varkappa$, γ, ε, ϱ, τ and σ. In addition to these, some of the alloy samples studied also show the θ-phase (silicon).

The liquidus surface maximum for the η-phase was found to be 860° (alloy 80).

The melting point of ϱ is 820° in the binary Cu-Mg system [17]. Increasing amounts of Si in solid solution raise it, and the maximum lies at a composition of about 7.5 % Si, 16.5 % Mg. The highest melting point recorded in the present work is 941°, alloy 262. The micrographs of this alloy (fig. 21) show traces of low-melting, Mg-rich constituents, and it is thus somewhat displaced from the true maximum point.

The maximum point in the region of the liquidus surface with the α-phase solidifying primarily from the melt is the melting point of pure copper, 1 083°.

b) *Ternary reactions with a liquid phase*

It is convenient to divide these reactions into two groups, according to alloy composition. The first comprises the reactions connected with the formation of the ternary τ- and σ-phases. The second group includes the transition reactions of the high-temperature phases from the binary system Cu-Si (Table VIII).

From the liquidus surface maximum point of the ϱ-phase (II: 3a), the liquidus temperatures diminish both with increasing Si contents and increasing Mg contents, more steeply in the former case (fig. 11). As the alloy composition nears 10 % Si with 19 % Mg, the samples contain progressively more of the τ-phase. With still more Si or Mg, as in alloy 265, low-melting constituents appear. No eutectic is formed by the ϱ- and τ-phases.

In ternary systems in general, there are three types of reactions which result in the formation of a new, *ternary* phase:

1) $A + B + \text{liq.} \leftrightarrows C$ (the melting point of C is lower than that of A or B)
2) $A + B \leftrightarrows \text{liq.} + C$ (the melting point of C is higher than that of A or B)*)
3) $A + \text{liq.}_1 \leftrightarrows C$ (the melting point of C is lower than that of A)
   $A + \text{liq.}_2 \leftrightarrows C$

In this case, the shape of the liquidus surface with only one maximum point (ϱ) precludes the possibility of reaction (1). τ obviously has a lower melting point than ϱ. This leaves a reaction of type (3) as the only possible solution.

There are two branches of the line of twofold saturation, which meet at a maximum point, M. The equilibrium reaction at this point is:

$$A + \text{liq. } M \leftrightarrows C$$ (ref. [41], p. 347).

The composition of phase C lies on a straight line between A and M in the basal projection.

Phase A is in this case represented by ϱ, and the equilibrium temperature (M) = 930°. This value is concluded from the results of the thermal analyses for the alloys 257 and 264, which show a thermal arrest at 929—930°. Alloy 265 (m.p. 928°) is obviously situated just off the point M. This will be given a new symbol, P_1.

The τ-reaction is thus found to be:

$$\varrho + \text{liq.} \leftrightarrows \tau \quad (P_1,\ 930°)$$ (Table VIII).

*) Reactions of this type are common in ternary systems with salt solutions, as for instance $Na_2SO_4 - ZnSO_4 - H_2O$ (ref. [41], p. 442).

TABLE VIII.

Four-phase equilibria in the copper corner of the ternary Cu-Mg-Si diagram

		Temp.	% Si	% Mg
P_1	$\varrho + \text{liq.} \leftrightarrows \tau$	930°	~ 10.9	~ 18.5
P_2	$\varrho + \tau + \text{liq.} \leftrightarrows \sigma$	826°	~ 14.3	~ 11.1
P_3	$\beta + \delta + \text{liq.} \leftrightarrows \gamma$	806°	8.9	0.7
P_4	$\delta + \gamma + \text{liq.} \leftrightarrows \varepsilon$	772°	9.3	1.65
T_1	$\beta + \text{liq.} \leftrightarrows \alpha + \varkappa$	824°	~ 7.3	~ 0.9
T_2	$\beta + \text{liq.} \leftrightarrows \varkappa + \gamma$	800°	8.4	0.9
T_3	$\delta + \text{liq.} \leftrightarrows \eta + \varepsilon$	763°	9.4	1.85
T_4	$\varepsilon + \text{liq.} \leftrightarrows \eta + \gamma$	745°	9.3	2.5
T_5	$\alpha + \text{liq.} \leftrightarrows \varkappa + \varrho$	718°	~ 7.1	~ 4.3
E_1	$\text{liq.} \leftrightarrows \eta + \sigma + \theta$	739°	13.7	4.8
E_2	$\text{liq.} \leftrightarrows \varrho + \eta + \sigma$	723°	10.7	7.1
E_3	$\text{liq.} \leftrightarrows \eta + \gamma + \varrho$	701°	8.8	3.85
E_4	$\text{liq.} \leftrightarrows \varkappa + \gamma + \varrho$	693°	7.6	3.9
	$\varkappa \leftrightarrows \alpha + \gamma + \varrho$	609°	~ 6.7	~ 1.5

The conditions for the σ-phase reaction are different from those mentioned above. There are now two solid phases present, ϱ and τ, which both have higher melting points than the new phase, σ.

The alloys 238 and 233 show a peritectic type thermal arrest, susceptible to supercooling, at 825°. This is also shown, at 826°, by alloy 247, which consists chiefly of τ-phase. The twofold saturation line representing the reaction $\varrho + \text{liq.}_2 \leftrightarrows \tau$ slopes down towards the second quaternary point P_2. As both ϱ and τ are present in the alloys above this point, the reaction must be a ternary peritectic one, conforming to type (1), as mentioned above:

$$\varrho + \tau + \text{liq.} \leftrightarrows \sigma \quad (P_2,\ 826°).$$

Two lines of twofold saturation start from the point P_2. One of these runs roughly in the direction of the line σ—θ (alloy 224, thermal arrest at 787°). The other branch runs nearly in the σ—η-direction at first. Alloy 207 exhibits the peritectic type of thermal arrest at 818°, and then a ternary eutectic solidification is suggested by the third thermal arrest at about 726°. The alloys 223 and 209 also have a marked secondary heat effect, which is found at progressively lower temperature levels, and alloy 231 shows only the ternary eutectic. There is thus primary solidification of the ϱ-phase, then the σ-reaction when the twofold saturation line is reached, and finally eutectic solidification (E_2 at 723°). This suggests that the line of twofold ϱ—σ-saturation has an inflexion point before reaching the eutectic point E_2 (fig. 18), and the solidification reaction thus changes from a peritectic to a eutectic one.

The reactions belonging to the *second group* are derived from three of the four*) equilibria in the binary system Cu-Si, viz.:

$$\alpha + \text{liq.} \leftrightarrows \beta \quad (852°)$$
$$\beta + \text{liq.} \leftrightarrows \delta \quad (\sim 826°), \text{ and}$$
$$\text{liq.} \lesssim \delta + \eta \quad (820°).$$

The reactions involving the β-phase will be considered first:

The line of twofold α—β-saturation starts from 7.6 % Si at 852° (system Cu-Si). The alloys 39 and 40 show the liquidus point values of 862° and 865°, respectively, on the surface of primary α-solidification. Alloy 44 (7.88 % Si, 0.11 % Mg), liq. point 851°, is found to be in the region of primary β-solidification. For the corresponding composition, 7.88 % Si, in the binary Cu-Si alloys, the value is 847° (by interpolation). Between 39 and 44 is alloy 41 with a liq. point of 829°, and showing a thermal arrest at 824° (fig. 14).

With somewhat higher Si contents than in the alloys 44 (above) and 47 (8.0 % Si, 0.54 % Mg; 844°), the liquidus temperatures of the alloys with primary β-solidification decrease. The surface of primary β-solidification terminates in a line of twofold β—δ-saturation, starting at 8.8 % Si and $\sim$ 826° (system Cu-Si).

When the Mg content in the alloys with 7.5 to 8.4 % Si is increased to 0.8 % and over, the $\varkappa$-phase solidifies primarily from the melt, and appears as an alloy constituent. The line of twofold β—$\varkappa$-saturation forms a maximum (about 835°, the solidus value obtained for alloy 43). The branch which slopes towards lower Si-content values meets the line of twofold α—β-saturation in a quaternary point T_1; the reaction temperature is found to be 824° (alloy 41). The β-phase reacts with the melt in a ternary transition (2:2) reaction:

$$\beta + \text{liq.} \leftrightarrows \alpha + \varkappa \quad (T_2,\ 824°).$$

The liquidus points of the alloys 96, 97 and 98 (i. e. 849°, 853° and 847°, respectively) show that in the region with primary $\varkappa$-solidification there is a slight maximum in the liquidus surface. These alloys show solidus point values near that of the ternary eutectic (E_4). This is also in agreement with the corresponding microstructures.

The development of the β—δ-reactions with increasing Mg content in the alloy samples is shown diagrammatically in fig. 16.

The line of twofold β—δ-solidification ends at a ternary peritectic point P_3 at 806° (alloys 55, 56, 61, 62). With still higher Mg contents (over 0.7 %), the γ-phase solidifies primarily from the melt (alloy 59, 827°). γ is thus formed peritectically in a 3:1 reaction:

*) The fourth, liq. $\leftrightarrows \eta + \theta$ (802°), is considered later in connection with the ternary eutectic E_1 (II:3 c).

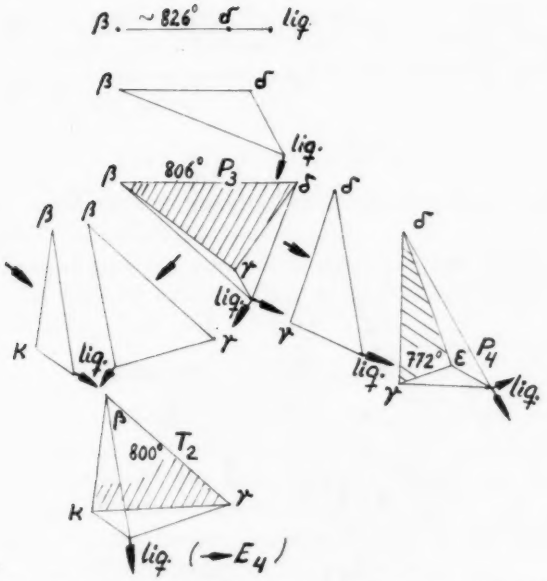

Fig. 16. Development of the β—δ-reactions (diagrammatically).

$$\beta + \delta + \text{liq.} \leftrightarrows \gamma \quad (P_3,\ 806°).$$

The microstructures of the alloys with primary γ-solidification, as in 141 and 144, are easily distinguishable from those with primary $\varkappa$ (II: 4).

From P_3, there descends a short line of twofold β—γ-saturation, which meets the β—$\varkappa$-branch sloping downward (with increasing Si contents) from the β—$\varkappa$-maximum point. The intersection point T_2 is placed at 800° (alloys 49, 51 and 58). The ternary transition reaction is:

$$\beta + \text{liq.} \leftrightarrows \varkappa + \gamma \quad (T_2,\ 800°).$$

The high-temperature β-phase has thus disappeared from the liquidus surface at temperatures lower than 800°, through the two 2:2 transition reactions T_1 and T_2.

The development of the δ—η-reactions with increasing Mg content in the alloy samples is shown diagrammatically in fig. 17.

The δ-phase solidifies primarily from the melt in the region between 9 and 10 % Si, 0 to 1.6 % Mg (fig. 15). The liquidus temperatures rise slightly with small additions of Mg; e.g. alloy 66, 0.22 % Mg, 826°, and alloy 73, 0.24 % Mg, 824°.

The line of twofold δ—γ-saturation descends from P_3 and ends at another ternary peritectic point, P_4, at 772° (alloys 109, 112, 113). The reaction is:

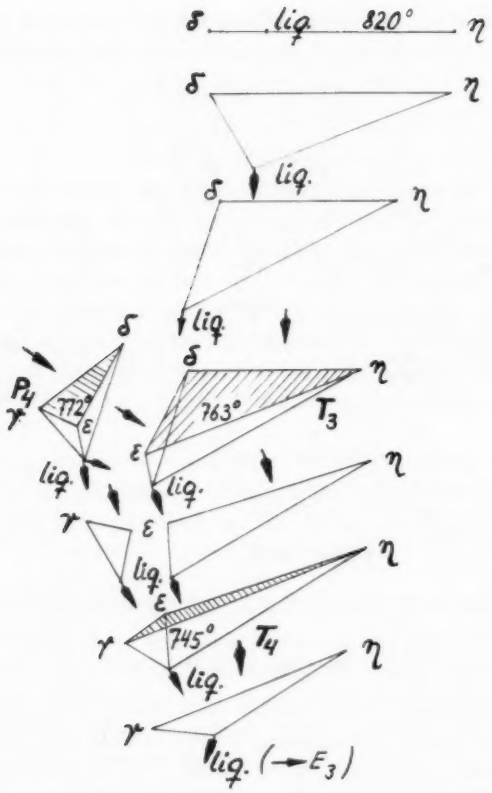

Fig. 17. Development of the δ—η-reactions (diagrammatically).

$$\delta + \gamma + \text{liq.} \leftrightarrows \varepsilon \ (P_4,\ 772°).$$

The line of twofold δ—η-saturation also has an inflexion point (fig. 19: change from eutectic to peritectic solidification reaction). It starts at 9.8 % Si and 820° (the δ—η-eutectic in the binary system Cu-Si), and meets the short δ—ε-branch descending from P_4 in a point T_3, 763° (alloys 74, 75, 76). Here δ reacts with the liquid phase:

$$\delta + \text{liq.} \leftrightarrows \eta + \varepsilon \ (T_3,\ 763°).$$

The thermal effects recorded here are the greatest observed in the present work. There is considerable supercooling if the cooling rates are increased. With the reaction T_3, the high-temperature δ-phase disappears from the liquidus surface.

There thus exists a small region (fig. 14) where the ε-phase can solidify primarily from the melt (alloys 147 and 149). The thermal arrests in the alloys 110, 147, 149 and especially 150 point to the following ternary transition reaction taking place at 745°:

$$\varepsilon + \text{liq.} \leftrightarrows \eta + \gamma \ (T_4,\ 745°).$$

The thermal arrest of the liquidus points in the alloys 147 and 149 almost coincide with those of the reaction T_4.

The only other alternative possibility would be the disappearance of the η-phase as the ternary eutectic (E_3) is approached along the line of twofold η—ϱ-saturation, i. e.:

$$\eta + \text{liq.} \leftrightarrows \varepsilon + \varrho \ (720°—705°?).$$

Alloys with η or ϱ solidifying primarily from the melt do not show any definite thermal arrests corresponding to this hypothetical reaction (alloys 152, 168, 169). In the alloys 167 and 179, which belong to the regions of primary γ- and ϱ-solidification, respectively, traces of η are revealed by X-rays (obviously from the ternary eutectic E_3). It is concluded that the reaction is the 2:2 transition reaction T_4, as above.

Thus the region of primary ε-solidification ends at T_4 (fig. 14), and represents only a very small part of the liquidus surface as compared even with the corresponding β- and δ-phase areas.

The line of twofold α—ϱ-saturation (fig. 11) starts at the eutectic point (722°, 9.7 % Mg) in the binary system Cu-Mg. It meets the line of twofold α—$\varkappa$-saturation, which is descending from point T_1, at a point T_5, at 718° (alloys 136, 177, 180). The ternary transition reaction is:

$$\alpha + \text{liq.} \leftrightarrows \varkappa + \varrho \ (T_5,\ 718°).$$

The approximate alloy composition values for the various quaternary points are included in Table VIII.

c) *Saddle surfaces and ternary eutectic points*

For alloys with low Si contents near the binary Cu-Mg boundary, the liquidus surface is saddle-shaped, the saddle point being on the line of twofold α—ϱ-saturation at about 760° (Si = 3.2 %, Mg = 6.8 %). The nearest values are obtained from the thermal analyses of alloys 218 (752°), 176 (744°) and 201 (741°), respectively (fig. 11).

The line of twofold β—$\varkappa$-saturation was found to have a saddle point at about 835° (II: 3b, alloy 43). It is located at approximately Si = 7.7 %, Mg = 0.7 % (fig. 14).

Between the ternary eutectic points E_3 and E_4, a saddle point was found at Si = 8.3 %, Mg = 3.8 % (alloy 164, 711°). It constitutes the maximum point of the line of twofold γ—ϱ-saturation.

The existence of a saddle point on the line of twofold η—ϱ-saturation is deduced from the solidus value of alloy 194 (722°). The ternary eutectic E_2 is on the other side of the straight line joining η and ϱ (alloy 198, 723°). The saddle point is located at approximately 10.4 % Si, 7 % Mg (fig. 11).

On the line of twofold η—σ-saturation, a corresponding saddle point was found between the ternary eutectic points E_1 and E_2, at about 770°, Si = 13 %, Mg = 5 %. The nearest values are obtained from the alloys 124 (750°) and 189 (763°). The composition of the latter is practically on the twofold saturation line.

The following four ternary eutectic points were found (Table VIII):

1) liq. $\leftrightarrows \eta + \sigma + \theta$ (E_1, 739°, fig. 11). Alloy 183.

The line of twofold η—θ-saturation, starting at 16 % Si and 802° in the binary system Cu-Si, slopes down to E_1. The other twofold saturation lines joining E_1 are from the η—σ saddle point, and from a corresponding point obviously existing on the pseudo-binary line σ—θ (cf. fig. 40).

2) liq. $\leftrightarrows \varrho + \eta + \sigma$ (E_2, 723°). Alloy 198.
3) liq. $\leftrightarrows \eta + \gamma + \varrho$ (E_3, 701°). Alloys 179, 144, 151.
4) liq. $\leftrightarrows \varkappa + \gamma + \varrho$ (E_4, 693°). Alloy 173.

The approximate compositions of the eutectic alloys are given in Table VIII.

d) *Metastable conditions during alloy solidification*

Some thermal effects obtained with alloys with primary δ-, η- or γ-solidification are caused by incomplete reactions with the liquid phase. For cooling rates greater than 2 degrees per minute, the reactions P_4, T_3 and T_4 are often suppressed, or at least appreciably supercooled. There follows a non-equilibrium reaction in which the excess liquid phase solidifies at temperatures about 678°—682° (fig. 13).

The apparent solidification of these alloys takes place as suggested by the diagram in fig. 20. It is a projection on the basal plane of the »liquidus surface» of *metastable* alloy composition. The supercooled solidification is observed in alloys belonging to the shaded area in fig. 20.

e) *Ternary reactions in the solid state*

The τ/τ'-transformation at 870° to 880° was not observed during the thermal analysis of samples containing the τ-phase (alloys 264, 266, 247).

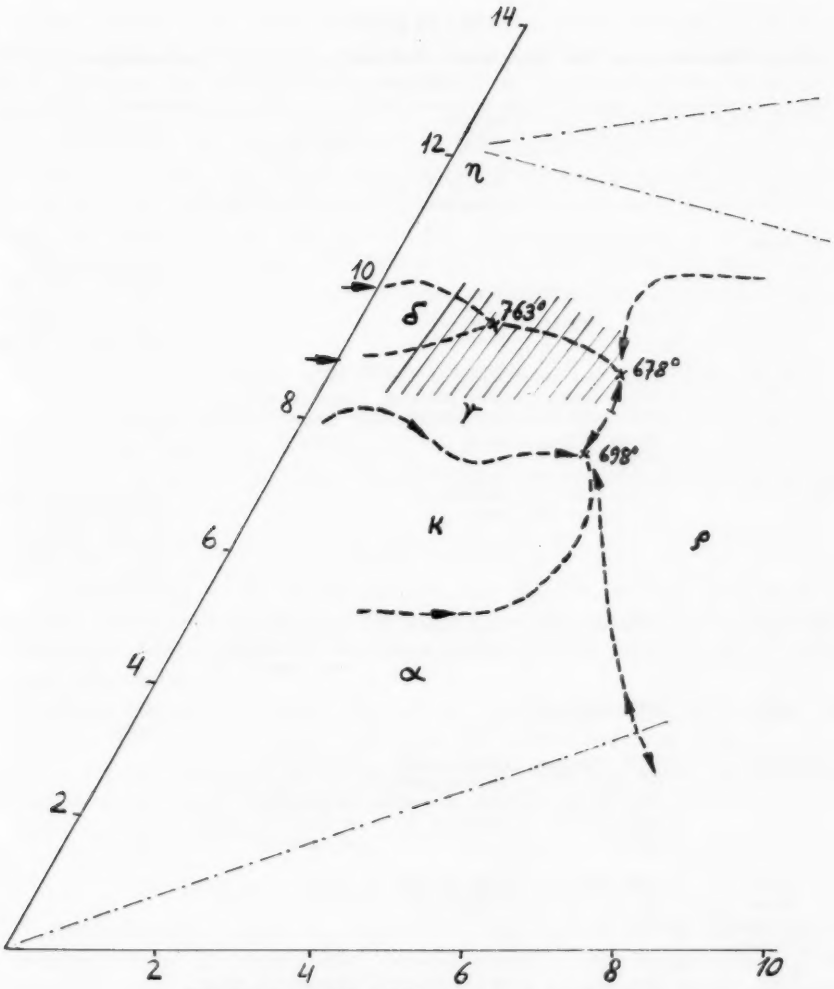

Fig. 20. Metastable solidification in the γ—δ—η-area.

In the ternary system, the kappa-phase decomposes eutectoidally according to the reaction:

$$\varkappa \leftrightarrows a + \gamma + \varrho \text{ (Appendix B, alloy 180).}$$

For the purpose of determining the eutectoidal temperature, powder samples from the alloys 137 and 139 were quenched from temperatures in the range of 550° upwards. It is evident that the $\varkappa$-phase is essentially stable at least at 620° (Appendix B, alloy 138).

TABLE IX

Etching characteristics and appearance of ternary constituents (microscopical examination).

Phase	Unetched	Etched: a b c (I: 5)	Primary crystals	Eutectic structures	Transformation structures
α	Pink to yellow (with more Si)	Etches slightly (c)	Slightly rounded dendrites	$\alpha + \varrho$ is coarse with rounded blocks of ϱ	—
β	Light	Not etched	—	—	Small dark loops in decomposition structure near T_2
$\varkappa$	Yellow	Dull yellow (c)	Elongated dendrites	see: γ	Fine $\alpha + \gamma$-structure after annealing
γ	Light	Light blue stain (a), to glossy white (with more Mg in solid solution)	Hard, in relief after polishing in 2- & 3-phase fields	Bluish feathery eutectic with $\varkappa$. Ternary E_4 etches brown (a)	—
δ	Light	Light and grey grains (a)	Medium hard	—	Faint lamellar type decomposition structure near P_2. Small dark rodlike blocks from δ/ε-reaction
η	Light	Light grey (a)	Very hard, rounded blocks	Characteristic $\eta + \varrho$-eutectic; same type in E_3	—
ε	Light	Dull yellow (a)	—	—	Small rounded blocks.
ϱ	Light	Light blue-grey to yellowish (with more Si); darker after anneal	Characteristic watered surfaces in 2- & 3-phase fields (a), (b)	Hard double-arrowhead dendrites or needles with α or $\varkappa$. Eutectic brown to dark (a)	—
τ	Light (bluish grey in fracture surfaces)	Light blue (a)	Long needles or platelets	—	—
σ	Light (bluish from polishing)	Clear blue (a), (b)	Jagged square or octagonal platelets	Etchant (b) stains $\eta + \sigma$-eutectic dark	—
ν	—	Red to dark brown in $\varrho + \nu$-alloys (a)	—	Component eaten, or stained black in eutectic (a)	—
θ	Blue-grey	Grey with magenta tint (a)	Small hard platelets	Darker than $\eta + \sigma$-eutectic in ternary eutectic E_1.	—
λ	Silvery gloss, corrodes in air to black	Dark (corroded) in 1 to 2 min. after etching (a)	Rounded blocks	Corroded after etching	—

The samples were first annealed at 450° in order to obtain complete decomposition of the $\varkappa$-phase, and were then quenched after a short anneal from temperatures slightly above 600°. The first appearance of the characteristic $\varkappa$- (01.0)-diffraction line at $\Theta = 20$ degrees is much easier to detect than the final $\varkappa$-decomposition in alloys with large amounts of the γ-phase present (Appendix C). While the powder photographs for 605° were still without $\varkappa$-diffraction lines, the samples quenched from 609° (alloy 137) and 612° (alloy 139) already showed the presence of $\varkappa$.

The alloys 37, 95 and 137 showed faint thermal arrests at 609° which are attributed to the eutectoidal $\varkappa$-decomposition (Appendix A). Table VIII.

4. Microstructures

The etching characteristic and appearance of the various constituents are given in Table IX. The etching reagents were acid ferric chloride (a), citric acid solution (b), and the modified ammonia-hydrogen peroxide reagent (c); cf. I: 5.

a) *The ϱ-phase*

Alloy 262 (Si = 7.8 %, Mg = 17.1 %), fig. 21. Almost homogeneous ϱ-phase nearly satured with Si. The micrograph shows some casting porosity (dark) and oxide inclusions, and traces of a Mg-rich constituent (ν) in the grain boundaries.

Alloy 251 (Si = 2.86 %, Mg = 15.7 %), annealed at 450°. Fig. 22. A hypereutectic $\alpha + \varrho$-alloy with about 16 % Mg shows the α-phase as the softer matrix (yellow with reagent (a)) and the blocks of primarily solidified ϱ stained light grey. Alloy 258 (3.14 % Si, 16.5 % Mg) still shows a two-phase $\alpha + \varrho$-structure.

b) *α, $\varkappa$ and γ. The ternary eutectic E_4*

Alloy 138 (Si = 6.45 %, Mg = 2.24 %), fig. 23, shows the structure resulting from the eutectoidal decomposition of the kappa-phase. The specimen was annealed at 450° for 168^h. The micrograph shows the remnants of the original $\varkappa$ blocks*), and a fine $\alpha + \gamma + \varrho$ network (Colour Plate I).

Alloy 98 (Si = 7.66 %, Mg = 1.03 %), fig. 24. The $\varkappa + \gamma$-eutectic which solidifies along the corresponding twofold saturation line is shown as a grey matrix. The loops of ternary eutectic (E_4) have a darker tint than the matrix after etching. The small blocks are partly decomposed $\varkappa$ containing some α.

*) In the binary Cu-Si alloys, kappa decomposes very slowly on annealing unless thoroughly cold-worked. Alloys such as 138 and 98 are too hard for cold-working.

Alloy 139 (Si = 7.1 %, Mg = 2.09 %), fig. 25. When the specimen has been annealed at 550° for 810^h the $\varkappa$-phase has formed α (arrow). The former eutectic loops, containing ϱ, appear as rounded, dark blocks in the γ-matrix. The former $\varkappa + \gamma$-eutectic (globularized) in half-tone.

Alloy 165 (Si = 8.6 %, 3.5 % Mg). Primary blocks of γ in a matrix of $\gamma + \varrho$-eutectic. Colour Plate II.

c) *δ, η, and ε. The ternary eutectic E_3*

Alloy 73 (Si = 9.80 %, Mg = 0.24 %), chill-cast specimen, fig. 26. Etching with reagent a) reveals a duplex structure with δ (grey) and γ (light). The transformation of δ into $\varepsilon + \gamma$ was interrupted by the fast cooling, leaving small, dark pits in the surface, which are brought out by the etchant (a).

Alloy 112 (Si = 9.23 %, Mg = 1.4 %), fig. 27. Blocks of ε (grey), and secondary $\gamma + \varepsilon$-eutectic, with some loops of dark ternary eutectic (E_3). This latter somewhat resembles the $\alpha + \delta$-eutectoid in tin bronzes.

Alloy 111 (Si = 9.3 %, Mg = 1.08 %), fig. 28. This alloy, which originally contained δ, was annealed at 600°. The resulting structure is an ε-matrix with white secondary γ. Some traces of the metastable eutectic are also visible.

Alloy 81 (Si = 12.15 %, Mg = 0.26 %), fig. 29. Almost pure η-phase, containing some undissolved platelets of θ.

Alloy 170 (Si = 10.7 %, Mg = 3.65 %), fig. 30. Hard blocks of primary η in relief, with the characteristic lamellar $\eta + \varrho$-eutectic. Alloy 181 (Si = 10.20 %, Mg = 4.84 %), fig. 31. The microstructure after annealing at 450° shows ϱ (light grey) in a matrix of ε.

d) *The ternary compounds σ and τ. The ternary eutectic E_1*

Alloy 233 (Si 13.7 %, Mg = 11.3 %), fig. 32. This alloy consists mostly of σ, with primary dendritic blocks of ϱ, some pseudo-eutectic showing up dark. Two micrographs in colour of alloys 248 (Si = 9.6 %, Mg = 14.0 %), and 207 (Si = 12.3 %, Mg = 9.72 %) are shown in Colour Plates III and IV. The former alloy contains mostly ϱ, and the amounts of σ present increase with higher Si contents towards the peritectic point P_2.

Alloy 187 (Si = 13.31 %, Mg = 5.99 %), fig. 33. Here σ solidifies as jagged, primary crystals in a matrix of the $\eta + \sigma$-eutectic, which etches dark with reagent (b). It is stained light brown with etchant (a). Colour Plate V.

The microstructures of the σ-phase which have the least amounts of other constituents are found at the composition 14.25 % Si, 11.15 % Mg. Some θ is precipitated in the σ-alloys with a Si content in excess of this

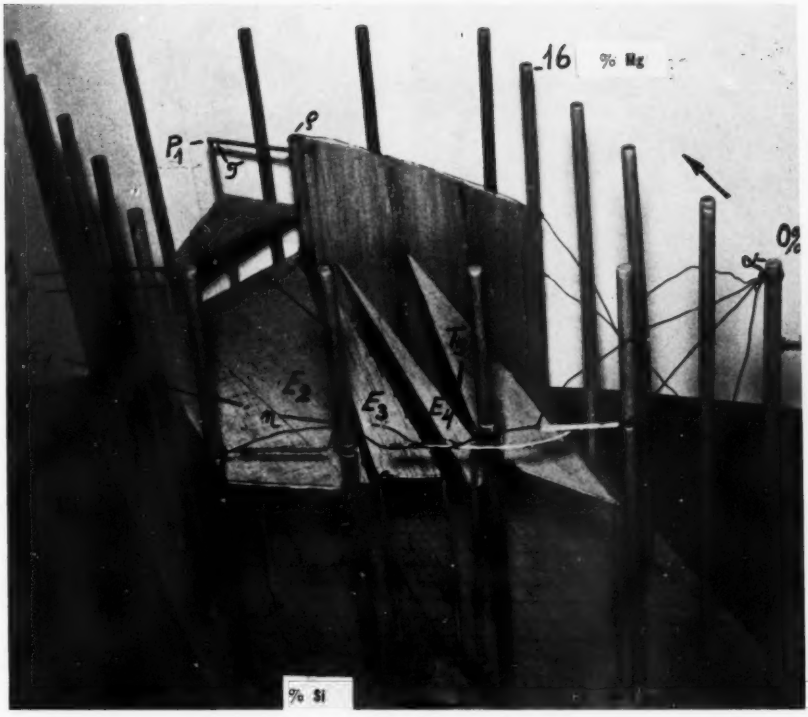

Fig. 12. Space model of the copper corner of the ternary diagram (0 to 16 % Si and Mg).

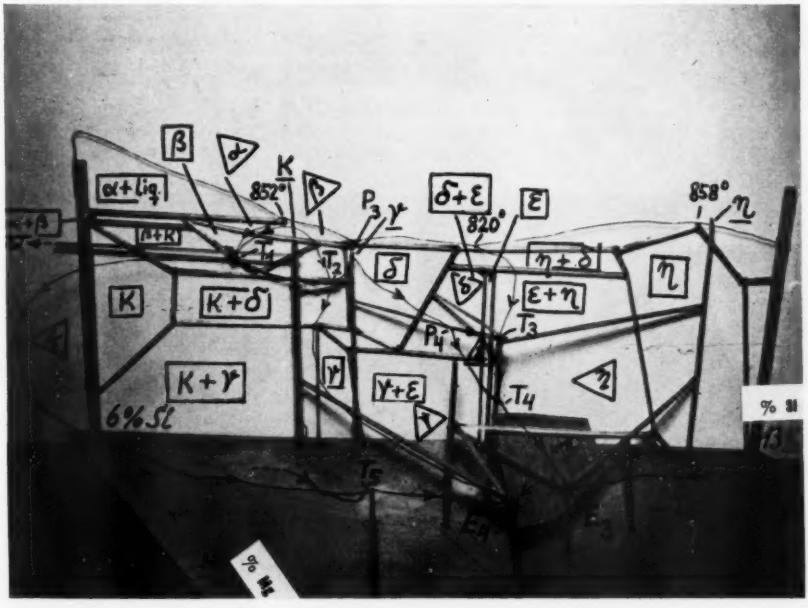

Fig. 13. Another space model, comprising the part from 6 to 13 % Si and 0 to 4 % Mg, which includes the ternary eutectic points E_3 and E_4.

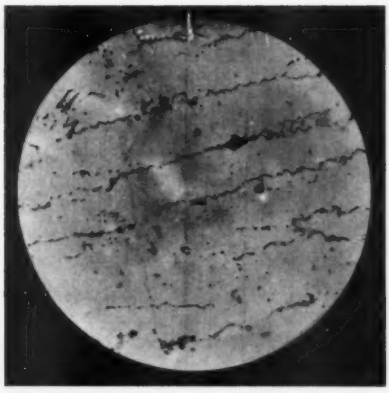

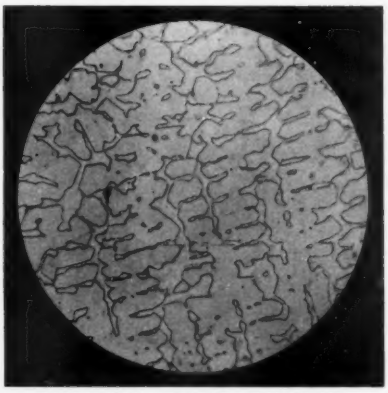

Fig. 21. The ϱ-phase, containing porosity and some oxide inclusions (dark), also a Mg-rich constituent (ν). Alloy 262, as cast, original magnification × 100.
Fig. 22. Hypereutectic $\alpha + \varrho$ alloy, annealed at 450°. Alloy 251, O.M. × 210.

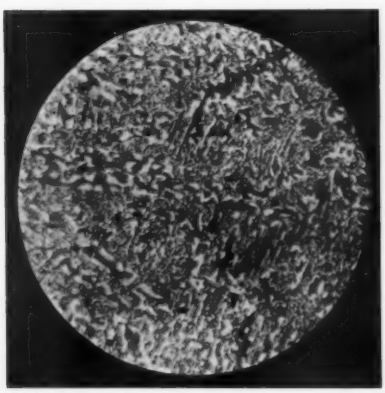

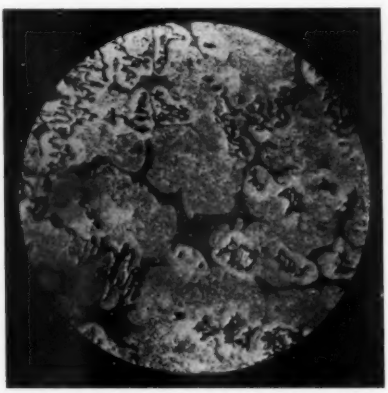

Fig. 23. Decomposing $\varkappa$ and fine $\alpha + \gamma + \varrho$ network. Alloy 138, annealed at 450° for 168h. O.M. × 500. Cf. Colour Plate I.
Fig. 24. The decomposition of $\varkappa$ leaves bright blocks of α, in low relief, surrounded by secondary γ (light), and the remainder of the original $\varkappa + \gamma$ -eutectic (half-tone). The dark loops are not visibly affected ternary eutectic (E_4). Alloy 98, annealed at 450°, O.M. × 460.

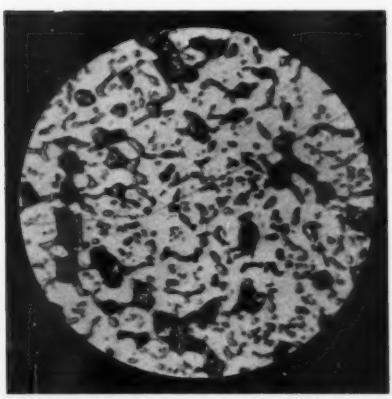

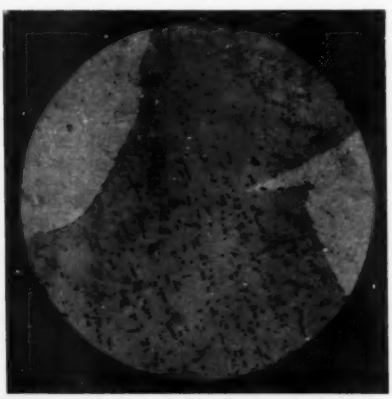

Fig. 25. Alloy 139, annealed at 550° for 810h. Double etch: c) + a). The former etchant has dissolved the remains of the ternary eutectic (dark). $\varkappa$ har formed α (arrow), and the matrix (light) is γ. The former $\varkappa + \gamma$-eutectic (globularized) in half-tone. O.M. × 500.
Fig. 26. Alloy 73, as cast. $\delta + \gamma$ (light). Starting δ-decomposition (dark spots). O.M. × 670.

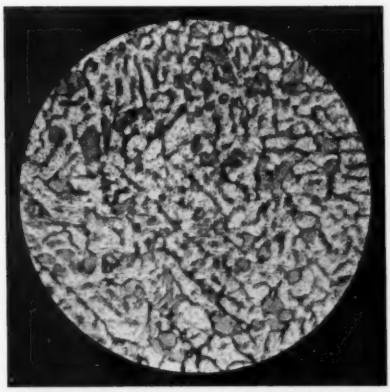

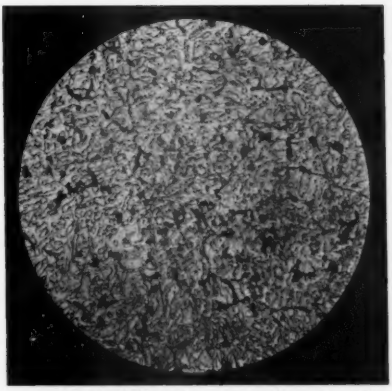

Fig. 27. Alloy 112, as cast. Primary (strictly taken secondary) solidification of ε (half-tone), with light γ and ternary eutectic E_3 (dark). O.M. $\times$ 280.
Fig. 28. Alloy 111, annealed at 600° (12h). Light γ in an ε-matrix, with traces of eutectic (dark). O.M. $\times$ 280.

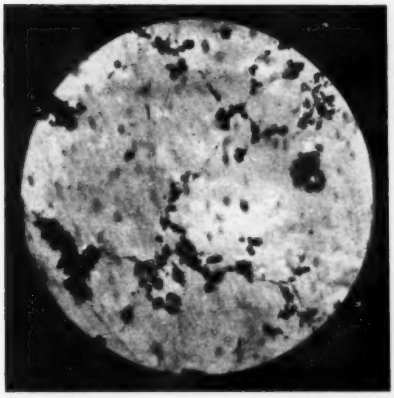

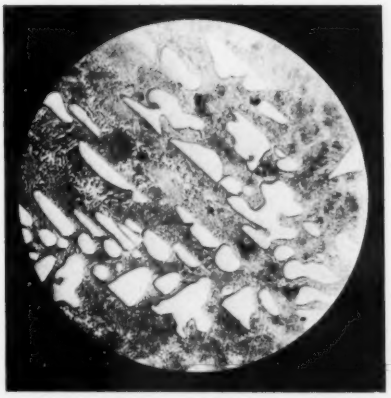

Fig. 29. Alloy 81, as cast. Almost pure η-phase, with some casting porosity and undissolved platelets of θ (grey). Unetched. O.M. $\times$ 500.
Fig. 30. Alloy 170, as cast. Primary blocks of hard, white η, with characteristic $\eta + \varrho$-eutectic. O.M. $\times$ 340.

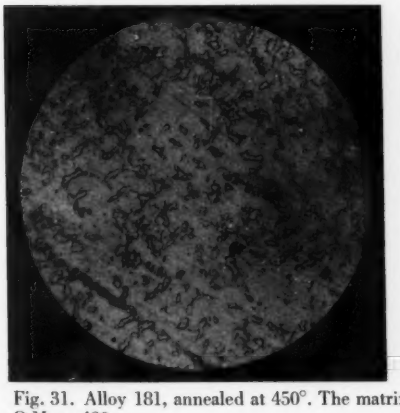

Fig. 31. Alloy 181, annealed at 450°. The matrix is ε, with some ϱ from the eutectic (light grey). O.M. $\times$ 420.
Fig. 32. Alloy 233. Light dendrites of primary ϱ, with σ as the matrix, and some traces of pseudo-eutectic in the grain boundaries. O.M. $\times$ 320.

COLOUR PLATE I.

Alloy 138, heat-treated at 450°. Primary $\varkappa$ decomposing into yellow α and light γ, with fine $\alpha + \gamma + \varrho$ network (appears brownish). O.M. × 360.

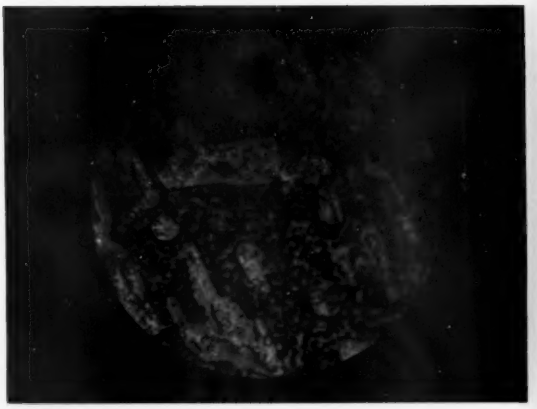

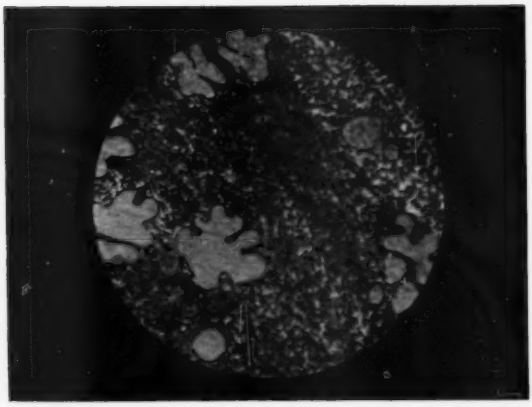

COLOUR PLATE II.

Alloy 135, showing a hypo-eutectic $\gamma + \varrho$ -structure, with white primary γ in a matrix of fine-grained eutectic. O.M. × 170.

COLOUR PLATE III.

Alloy 248. Small blue blocks of σ in a matrix of watered, light ϱ. O.M. × 170.

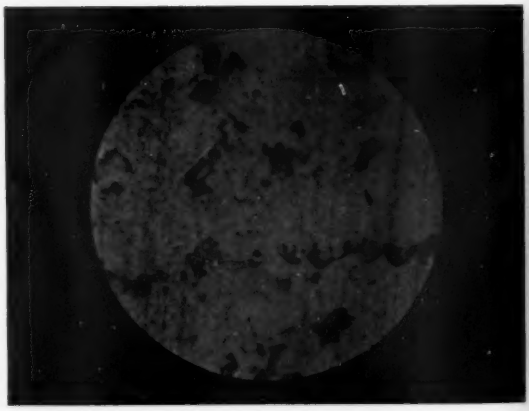

COLOUR PLATE IV.

Alloy 207. Blue σ-platelets with light ϱ, and traces of pseudo-eutectic stained dark. O.M. × 170.

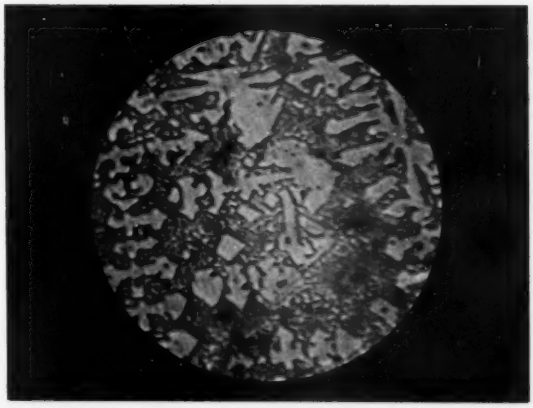

COLOUR PLATE V.

Alloy 187. Primary σ (light) as characteristically shaped crystals in a matrix of σ-η-eutectic. O. M. × 110.

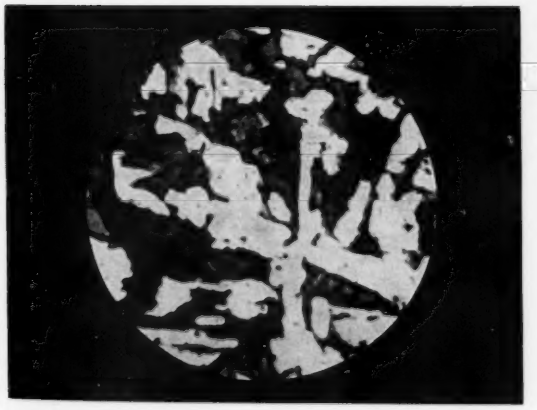

COLOUR PLATE VI.

Alloy 268. White blocks of primary τ, with ν ($CuMg_2$) light brown, and the Mg-rich pseudo-eutectic stained an iridiscent blue or corroded dark. O.M. × 170.

ALL COLOUR PLATES magnified about 2.7 times in reproduction.

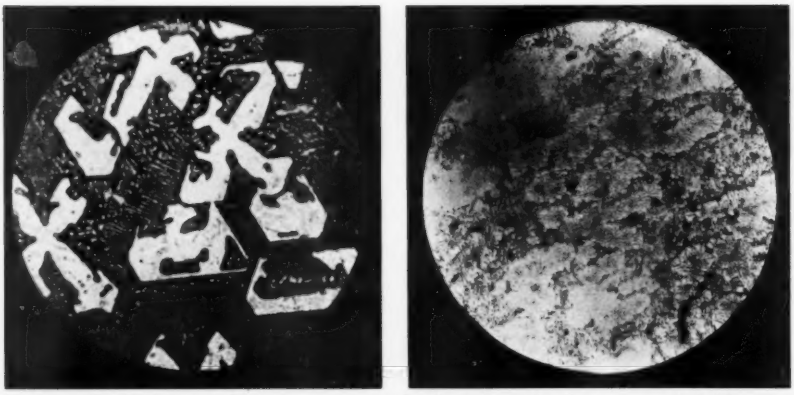

Fig. 33. Alloy 187, as cast. Jagged primary crystals of σ in a matrix of $\eta + \sigma$-eutectic (with some ternary eutectic E_2), etched dark with etchant b). O.M. $\times$ 320.
Fig. 35. Alloy 183. Primary crystallization of the θ-phase near the ternary eutectic E_1. θ as clusters of very small, dark inclusions in a matrix of light ternary eutectic. O.M. $\times$ 320.

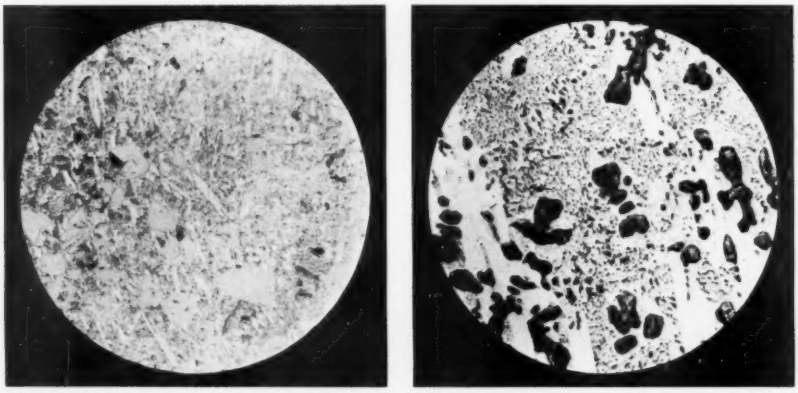

Fig. 36. Alloy 250, as cast. Large blocks of τ (grey), with coarse secondary σ (light), and $\tau+\sigma+\theta$—eutectic (E_5). O.M. $\times$ 120.
Fig. 37. Primary λ, corroded dark, and coarse columnar τ, with ternary eutectic $\lambda+\tau+\theta$ (E_6). θ in half-tone. Alloy 269, as cast. O.M. $\times$ 380.

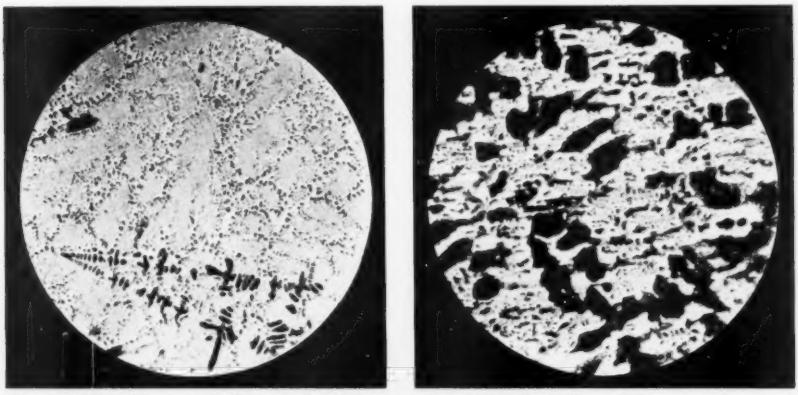

Fig. 38. Alloy 270, as cast. Primary λ and the ternary eutectic E_6. O.M. $\times$ 380.
Fig. 39. Primary τ (light), with some ν-phase (half-tone), and a dark, corroded pseudo-eutectic, whose composition has shifted over into the $\nu + \lambda + \mu$ field (transition reaction π, fig. 40). Alloy 271, O.M. $\times$ 190.

All micrographs, except Colour Plates, are reproduced in $\frac{2}{3}$ size. Etchant a) is used, except where otherwise stated.

Fig. 13:

LEGEND:

$\boxed{\beta}$, $\boxed{\delta}$, $\boxed{\varkappa+\delta}$,... etc. : 1- or 2-phase areas in the binary equilibrium diagram (Cu-Si)

$\underline{\varkappa}$, $\underline{\chi}$, $\underline{\eta}$: phases in the ternary system Cu-Mg-Si, in ternary equilibria, e.g.:
$\beta + \delta +$ liq. $\rightleftarrows \gamma$
(ε is not shown in the space model)

$\triangle\!\!\!\!\!\!\varkappa$, $\triangle\!\!\!\!\!\!\delta$,... etc. : surfaces of primary $\varkappa$-, δ-, etc., crystallization in the ternary system.

M Plane below E_3 represents metastable solidification at about 678° (cf. fig. 20).

value, and the amount of θ can be determined separately during the chemical analysis. In fig. 34, the shaded area represents alloy compositions where precipitation of θ can be detected in this way. The region of optimum σ-content is somewhat offset from the stoichiometrical composition $Cu_{16}Mg_6Si_7$, because of the peritectic-type reaction in P_2 (cf. WITTE [31], and NAGORSEN and WITTE [32]).

In the $\varrho + \tau$-alloys, τ solidifies as light-coloured needles or platelets.

Alloy 183 (Si = 13.95 %, Mg = 4.15 %), fig. 35. The micrograph shows the microstructure near the eutectic point E_1, with a small amount of θ, stained dark, and the light eutectic containing chiefly σ and η.

e) *The Si- and Mg-rich areas*

Some alloy samples with high Si and Mg contents were melted, and these also showed constituents other than η, σ or τ. The microstructures were compared with the results of earlier research [29]. Because of the high Mg contents, no heat treatment or thermal analysis was attempted on this series of alloys.

The alloys 250, 267, 268, 269, 270 and 271 (fig. 40) were studied microscopically, and in part also by means of X-rays.

The microstructures of the alloys 267 (Si = 11.32 %, Mg = 27.90 %) and 268 (Si = 9.45 %, Mg = 28.4 %) show the light τ-blocks with ν, which etches reddish brown with etchant (a), and a dark or iridiscent, Mg-rich pseudoeutectic (Colour Plate VI). This latter is excessively corroded by the etching reagents, and immersions of only 1 sec. duration still gave deep pits in the polished surface.

The X-ray results for the alloys 250 and 269 to 271 were as follows:

250	Si = 25.86 %	Mg = 14.12 %	$\tau + \sigma$
269	25.15	23.12	$\tau + \lambda$
270	18.85	27.88	$\tau + \lambda$
271	14.71	34.72	$\tau + \lambda + \nu$

The alloys 250, 269 and 270 also contain 12.0, 7.25 and 0.65 %, respectively, of the θ-phase, as revealed by chemical analysis.

Alloy 250, fig. 36. Large primary blocks of τ, some coarse secondary σ (light), and a fine-grained eutectic (stained yellow) containing τ, σ and the magenta-tinted θ (dark in the micrograph).

The alloys 269 and 270 (fig. 37, 38) contain primary λ (dark) in a fine-grained eutectic of $\tau + \theta + \lambda$.

Alloy 271 (fig. 39) has a fringe of brownish ν (grey in the micrograph) around the primary blocks of τ (light), and a dark, corroded, Mg-rich pseudoeutectic.

III. DISCUSSION

In the ternary system Cu-Mg-Si there exist only the two previously known ternary compounds, τ and σ. There are no known solubility gaps in the liquid state nor any allotropic transformations of the metal phases. The character of the copper corner of the diagram is thus influenced mainly by the complicated equilibria in the binary system Cu-Si, involving 7 intermediate phases.

1. The isothermal section at 450° C

a) *The copper corner of the diagram*

The following factors are to be noted in connection with this part of isothermal section:

— the solid solubility of Si in the σ-phase (II: 1c, II: 2b), which could also be inferred from the results of WITTE [31];

— the disappearance of the high-temperature phases β, $\varkappa$ and δ. Taking $\varkappa$ as an example, the present work shows that additions of Mg raise the lower temperature limit of the $\varkappa$-phase by 54°. The β-phase is not stabilized by additions of Mg*). Cf. Table X;

— the existence of the two ternary compounds, τ and σ, and their narrow ranges of solid solubility [29, 31].

τ and σ, with the ϱ-phase, form a »boundary» between the copper corner and the rest of the diagram. This is evident on comparing the basal projection of the system Cu-Mg-Si with that of Al-Mg-Si, for instance, which has a pseudo-binary section from the Al corner to Mg_2Si, or Cu-Mg-Sb, which has only the ternary compound CuMgSb [42].

— the ε-phase can coexist at 450° with ϱ and σ in two- or three-phase fields, even where the alloys after solidification contain η and no ε. This can be explained by a solvus-type reaction in the solid state, as the range of solid solubility for ε increases considerably when the temperature is lowered (fig. 10, 450°). This reaction has not been confirmed by thermal analysis, however;

*) WITTE [30] had succeeded in retaining the high-temperature τ-phase ($MgNi_2$ type, stable above 870°) at lower temperatures by adding Al to the alloy composition.

— the ε-phase does not coexist with the θ-phase (cf. alloy 124, 183, Appendix B). The hypothesis of a possible three-phase $\varepsilon + \sigma + \theta$ field has not been confirmed;

— PORTEVIN and BONNOT [29] held that the section η—τ is pseudo-binary (fig. 4 A), but they were not aware of the existence of the σ-phase. The section η—σ might be considered pseudo-binary, but for the slight solid solubility range of the η-phase.

b) *The Si- and Mg-rich areas*

PORTEVIN and BONNOT [29] had discovered the two pseudo-binary sections τ—λ and τ—ν. In the present work, it is deduced from the X-ray examination of the alloys 250, 269, 270 and 271 (II: 4e, and Appendix B) that there exist two more, viz. τ—θ and σ—θ. These are included in fig. 40, which represents a projection of the pseudo-binary sections and some of the lines of twofold saturation on the base plane of the diagram.

In fig. 40, the section $MgCu_2$—»$MgSi_2$» used by WITTE [31] is drawn as a broken line. It is, of course, not a pseudo-binary section, but a line of constant Mg content (33 atomic per cent).

2. The liquidus surface in the Si- and Mg-rich areas

The directions of the lines of twofold saturation near the alloys 250, 269, 270 and 271 can be approximately deduced from the amounts of eutectic found in the microstructures (fig. 40). Cf. II: 4e. There are two proposed ternary eutectic points, viz. in the three-phase fields $\tau + \sigma + \theta$ (E_5) and $\tau + \theta + \lambda$ (E_6). The former is tentatively placed at 731°, to accord with a thermal arrest obtained with the alloy 224 (Si = 16.1 %, Mg = 10.8 %).

The temperature (765°) of the minimum point of the section $MgCu_2$—»$MgSi_2$» is taken from the work of WITTE [31], and the corresponding point on the section τ—λ (857°) was determined by PORTEVIN and BONNOT [29]. The latter give 927° as the melting point of τ, while the value 930° (P_1) was found by the present author. This difference is insignificant, since small amounts of impurities may influence the temperature readings considerably.

It may be pointed out that the absence of a ternary eutectic or peritectic point in the three-phase field $\tau + \lambda + \nu$ is by no means an unusual feature of ternary systems. The ternary transition point π (508°) has been displaced to the other side of the line ν—λ, towards the ternary eutectic o (at 479°) in the three-phase field $\mu + \nu + \lambda$. The symbols π, o are those used by PORTEVIN and BONNOT.

The line of twofold ϱ—ν-saturation, starting at 550° in the binary system Cu-Mg, probably has a saddle point not far from the point corresponding to the composition $CuMg_2$ (ν). It is also concluded that this line, and that of twofold ϱ—τ-saturation (from P_1), meet at a point T_6, at about 540° (fig. 40):

$$\varrho + \text{liq.} \leftrightarrows \tau + \nu \ (T_6, \sim 540°).$$

The line of twofold τ—ν-saturation then continues towards the ternary transition point π at 508°, as in fig. 4 B.

3. The ternary equilibria

In section II: 3b, the three types of reactions in which a *ternary* phase (C) is formed were mentioned:

1) $A + B + \text{liq.} \leftrightarrows C$
2) $A + B \leftrightarrows \text{liq.} + C$
3) $A + \text{liq.}_1 \leftrightarrows C$
   $A + \text{liq.}_2 \leftrightarrows C$

In the case where phases from one of the binary systems also participate in reactions with the melt, a low-temperature phase can appear in the equilibria in the two following ways (corresponding to the reactions (1) and (3) cited above):

1) a ternary peritectic reaction $A + B + \text{liq.} \leftrightarrows C$ (3:1)
2) a reaction $A + \text{liq.} \leftrightarrows C$, which occurs at a saddle point on the line of twofold A—C-saturation. This is often followed by one or two ternary transition reactions, in which the A-phase disappears, e. g.:
2b) $A + \text{liq.} \leftrightarrows C + D$ (2:2).

The γ- and ε-phases are formed through reactions of type (1), and the β—$\varkappa$-transformation is an example of type (2). β then disappears through two transition reactions T_1 and T_2.

The ternary equilibrium reactions are arranged in Table X for comparison with the reactions in the binary system Cu-Si.

From Table X it can be seen that the formation temperature is substantially depressed only in the case of the ε-phase, when Mg is added to the Cu-Si alloys. The ε-phase is also different from the others in that the surface of primary ε-solidification is rather small, and closes at higher Mg contents (transition reaction T_4), although the solid solubility of Mg in the ε-phase is substantial at 450° (II: 2b). The evidence for the reaction T_4 is, however, conclusive (II: 3b).

TABLE X

Comparison of phase formation and decomposition temperatures in the binary system Cu-Si and the ternary system Cu-Mg-Si

Phase formation

Binary system (Cu-Si)			Ternary system (Cu-Mg-Si)		
Phase	Reaction	Temperature, °C	Reaction	Formation temperature °C	Maximum liq. temp. recorded' °C
β	$\alpha + \text{liq.} \leftrightarrows \beta$	852°			(851°)
δ	$\beta + \text{liq.} \leftrightarrows \delta$	830°			(826°)
$\varkappa$	$\alpha + \beta \leftrightarrows \varkappa$	842°	$\beta + \text{liq.} \leftrightarrows \varkappa$	835°	847°
γ	$\varkappa + \delta \leftrightarrows \gamma$	730°	$\beta + \delta + \text{liq.} \leftrightarrows \gamma$	806°	827°
ε	$\delta + \eta \leftrightarrows \varepsilon$	800°	$\delta + \gamma + \text{liq.} \leftrightarrows \varepsilon$	772°	—

Phase decomposition or transition

		Decomposition or transition temperature, °C		Decomposition or transition temperature, °C
α	$\alpha + \text{liq.} \leftrightarrows \beta$	852°	$\alpha + \text{liq.} \leftrightarrows \varkappa + \varrho$	718°
β	$\beta \leftrightarrows \varkappa + \delta$	784°	$\beta + \text{liq.} \leftrightarrows \alpha + \varkappa$	824°
			$\beta + \text{liq.} \leftrightarrows \varkappa + \gamma$	800°
δ	$\delta \leftrightarrows \gamma + \varepsilon$	710°	$\delta + \text{liq.} \leftrightarrows \eta + \varepsilon$	763°
$\varkappa$	$\varkappa \leftrightarrows \alpha + \gamma$	555°	$\varkappa \leftrightarrows \alpha + \gamma + \varrho$	609°

Additions of Mg raise the decomposition temperatures of the β-, δ- and $\varkappa$-phases (Table X). The reactions by which $\varkappa$ and ε are formed, and also those of β- and δ-decomposition, are different from those of the binary system Cu-Si. It is because the γ-phase appears in equilibrium with the melt at as low a Mg content as 0.7 % (for Si = 8.9 %) that the reactions between the $\varkappa$- and δ-phases cannot take place in alloys with Mg contents substantially higher than this.

An interesting feature is that the temperature level for the solid state reaction:

$$\varkappa + \delta \leftrightarrows \gamma \text{ (730°, binary system Cu-Si)}$$

is at first depressed by minute additions of Mg to about 712° (Appendix A, alloys 40 to 44). The effect is similar for the δ-decomposition:

$$\delta \leftrightarrows \gamma + \varepsilon \text{ (710°, binary system Cu-Si),}$$

which gives thermal arrests at about 686° in the alloys 65, 68 and 72 (with Mg contents up to 0.12 %). This type of effect is found within the range of solid solubility of Mg in the intermediate phases in question.

IV. SUMMARY

The copper corner of the ternary diagram Cu-Mg-Si has been studied by X-ray diffraction methods and thermal analysis. The results are presented in the form of an isothermal section at 450° C (fig. 10), and a projection of the liquidus surface on the basal plane of the diagram (fig. 11, with details in figs. 14 and 15). Some micrographs of alloys are included.

No hitherto unknown ternary phases have been found. The high-temperature phases β, $\varkappa$ and δ (binary system Cu-Si) disappeared in the isothermal section at 450°.

The four-phase equilibria and the ternary eutectic points found are presented in Table VIII.

Lattice parameter determinations were carried out with X-rays on samples with the ϱ-phase (Cu_2Mg) containing varying amounts of Si in solid solution. The lattice parameter value a = 7.030 Å diminishes to 6.969 Å at the saturation limit (about 7.8 % Si, in alloys in equilibrium with the α-phase).

Further investigation is needed in the cases of the β-, δ- and η-phase lattices.

A tentative model of the basal projection of the ternary system Cu-Mg-Si is depicted in fig. 40, on the basis of work by earlier authors augmented with the results of the present investigation.

References

1. M. Hansen: Aufbau der Zweistofflegierungen. I ed. Berlin 1936 (Book). Also: II ed. (with K. Anderko): Constitution of binary alloys. New York 1958.
2. C. S. Smith: J. Inst. Metals **40** (1928), 359—370.
3. C. S. Smith: Trans. AIME **51** (1929), 414—439.
4. C. S. Smith: Trans. AIME **137** (1940), 313—333.
5. S. Arrhenius and A Westgren: Z. phys. Chemie (B) **14** (1931), 66.
6. A. G. H. Andersen: Trans. AIME **137** (1940), 334—353.
7. W. B. Pearson: Handbook of lattice spacings and structures of metals and alloys. London 1958. (Book).
8. E. Voce: J. Inst. Metals **44** (1930), 331—361.
9. K. Sautner: Forschungsarbeiten der Metallkunde und Röntgenmetallographie, 1933, N:o 9.
10. T. Isawa: Nippon Kinzoku Gakkai-Si **2** (1938), 400, also **4** (1940), 398. A.
11. K. Iokibe: Kinzoku-no-Kenkuy (1931), 433—456. A.
12. K. Schubert: Z. Metallkunde **38** (1947), 349; **39** (1948), 88; **41** (1950), 417.
13. K. Schubert: Z. Metallkunde **43** (1952), 1—10.
14. K. Schubert and G. Brandauer: Z. Metallkunde **43** (1952), 262—268.
15. F. R. Morral and A. Westgren: Arkiv Kemi, Mineralogi, Geologi **11 B** (1934), 6.
16. M. Okomoto: Sci. Rep. Tôhoku Imp. Univ. (1) **27**, 155. A.
17. W. R. D. Jones: J. Inst. Metals **46** (1931), 395; **58** (1936), 41—48.
18. J. B. Friauf: J. Am. Chem. Soc. **49** (1927), 3107.
19. A. Runquist, H. Arnfelt and A. Westgren: Z. anorg. Chemie **175** (1928), 43.
20. G. Ekwall and A. Westgren: Arkiv Kemi, Mineralogi, Geologi **14 B** (1940), 7.
21. K. Schubert and K. Anderko: Naturwiss. **38** (1951), 46; also 259.
22. V. G. Sederman: Phil. Mag. **18** (1934), 343—352.
23. E. Zintl and A. Harder: Z. phys. Chemie (B) **16** (1932), 206. A.
24. F. Laves and H. Witte: Metallwirtschaft **14** (1935), 645.
25. R. Vogel: Z. anorg. Chemie **61** (1909), 46—53. A.
26. L. Wöhler and O. Schliephake: Z. anorg. Chemie **151** (1926), 11—20.
27. E. A. Owen and G. D. Preston: Proc. Phys. Soc. **36** (1924), 343—345.
28. W. Klemm and H. Westlinning: Z. anorg. Chemie **245** (1941), 365.
29. A. Portevin and P. Bonnot: Comptes rendus **196** (1933), 1603—1605.
30. H. Witte: Z. angew. Mineralogie **1** (1938), 255—268.
31. H. Witte: Metallwirtschaft **18** (1939), 459—463.
32. G. Nagorsen and H. Witte: Z. anorg. Chemie **271** (1952), 144.
33. N. P. Tucker: J. Iron and Steel Inst. **115** (1927), 412—416.
34. A. Cohen: Rationelle Metallanalyse. Verl. Birkhäuser, Basel 1948, pp. 147, 303. (Book).
35. K. J. B. Wolfe: Metal Treatment, Spring 1946, 25—35.

36. M. U. Cohen: R. Sci. Instruments **6** (1935), 68.
37. M. U. Cohen: Z. Krist. **94** (1936), 288.
38. M. J. Buerger: X-ray Crystallography, Wiley, New York 1942. (Book).
39. G. L. Kehl: Metallographical Laboratory Practice. McGraw-Hill, New York, 1943. (Book).
40. L. J. Aschan: unpublished research.
41. R. Vogel: Vol. II: Die Heterogenen Gleichgewichte, in: Handbuch der Metallphysik (G. Masing ed.), Leipzig 1937, pp. 437, 445. (Book).
42. E. Scheil and W. Sibert: Z. Metallkunde **33** (1941), 389.
43. H. Nowotny and H. Bittner: Monatsh. Chem. **81**, 1950, 887—906.

A = abstract only available as source.

Appendix A

Alloy composition and results of the thermal analyses.

Alloy No.	Composition %			Thermal analysis (readings in degrees C)	
	Si	Mg	Fe		
1	0.06	0.76	0.18		
2	0.52	.09	.06		
4	0.38	.42	.08		
5	0.47	.60	.07		
6	0.5	.8	.07		
7	0.51	.015	.05		
8	0.50	.04	.08		
9	0.52	.05	.11		
10	0.85	.06	.10		
11	0.86	.07	.10		
12	0.94	.10	.12		
13	0.94	.38	.13		
14	1.01	.06	.44		
15	1.00	.19	.13		
16	0.96	.61	.07		
17	0.37	.07	.07		
18	0.37	.09	.06		
19	0.37	.19	.07		
20	1.73	.15	.13		
21	1.83	.19	.14		
22	1.82	.21	.08		
23	1.83	.48	.08		
24	1.97	.66			
25	3.14	.42	.01		
26	3.69	.97	.02		
27	3.96	.09	.10		
28	3.85	.12	.14		
29	3.87	.20	.10		
30	3.98	.48	.10		
31	5.07	.39	.01		
32	5.11	.42	.01		
34	4.94	.93	.11		
35	5.52	.50	.01		
36	6.10	.79	.21	923/(778)/**703**	
37	6.60	.84		907/849/(672)/612)	
38	6.15	—	.23		
39	7.3	.15		862/**851**—847 sol./(780)/699	
40	7.12	.51	.01	865/829/(759)/**712**	
41	7.7	.15		829/824/**712**	T_1
42	7.60	.61	.10	835/(820)/765/**713**	
43	7.82	.48	.13	843/(835)/776/713	
44	7.88	.11	.22	851/(848)/835/780/720	
45	8.2	—	.39		
46	8.25	.34	.01	829/822/774/709	
47	8.0	.54		844/(831)/780/704	
48	8.39	.16	.02	824/(818)/709	
49	8.36	.43		826/**802**/785/(709)/(682)	
50	8.40	.64	.02	804/709	
51	8.67	.51	.03	807/**800** sol./693	T_2
52	8.75	.82		804/(800)/792(698)	
53	8.70	.88	.02	798/(793)/707	
54	8.97	.77		802/(800)/690	
55	8.89	.23		816/807/**703**	
56	8.90	.32	.02	811/805/797/**692**	P_3
57	8.90	.07		822/(**818**)/**686**	

Appendix A (cont.)

Alloy No.	Composition %			Thermal analysis (readings in degrees C)	
	Si	Mg	Fe		
58	8.8	0.69		805/(802)/**699**	
59	8.86	.86	0.02	827/807—804/**703**	
60	9.0	.17		**818**/(815)/695	
61	9.10	.43		815/(807)/715	
62	9.0	.58	.02	813/806/**705**/(697)	P_3
63	9.0	.64	.04	805/(705)/**693**	
64	9.21	—	.11	**824**/756/724	
65	9.25	.085		822/**818**/688	
66	9.23	.22		826/(818)/**712**	
67	9.26	.48	.02	816/806/(752)/(703)	
68	9.46	.12		(822)/818/(815)/(733)/**686**	
69	9.50	.65		813/802—798/(684)	
70	9.58	.86	.02	(813)/(804)/783/(737)/694	
71	9.82	—	.17	(822)/**819**/(808)/(722)/710	
72	9.78	.10		**820**/815/695/682	
73	9.80	.24	.04	824/817/(772)/**710**	
74	9.8	.93	.13	820/(818)/**757**/712	T_2
75	10.50	.66		826/**759**/714	T_3
76	10.85	.52	.04	846/840/**763**	T_3
77	10.83	.96		837/(761)/**754**/714	
78	11.65	.05	.01	860/833/(824 sol.)/(718)	
79	11.55	.17	.02	**853**/(844 sol.)/(757)/(712)	
80	12.15	.18	.02	860/855 sol.	
81	12.15	.26	.30	857/(841 sol.)	
82	7.98	.72		818/(763)/**714**	
86	0.08	1.75	.09		
87	1.01	.48	.07		
88	1.8	.24	.42		
89	2.49	.85	.10	998/748	
90	3.26	.15	.21		
91	3.97	.28	.08		
92	4.78	.16	.13		
93	5.32	.15	.02		
94	5.06	.13	.02		
95	6.30	.31	.02	(824)/780/701/(609)	
96	6.5	.42	.14	849/716/702 sol.	
97	6.93	.36		853/711	
98	7.66	.03	.23	847/726/701 sol.	
99	7.45	.63	.02	(816)/800/705/699	
100	7.87	.36	.02	813/780/(748)/716	
101	7.7	.52	.02	805/773/(743)/(687)	
102	7.70	.73	.02	805/735/727	
103	8.12	.45		785/(710)/(686)	
104	8.25	.57	.02	769/**699**	
105	8.66	.40	.01	787/703/684	
106	8.65	.95	.01	767/705/678	
107	8.99	.49	.17	783/703	
108	8.98	.50	.13	783/(697)/(682)	
109	9.13	.36	.03	806/**772**/(733)/695	P_4
110	9.05	.55	.03	787/741/703	T_4
111	9.30	.08	.17	811—791/(714)/686	
112	9.23	.4		789/(772)/699/684	P_4
113	9.30	.53	.01	778/(772)/735/**703** sol./(680)	P_4
114	9.38	.55	.02		
115	9.75	.16		802/(768)/(742)/(699)	
116	9.45	.76		767/(754)/**699**	E_2

Appendix A (cont.)

Alloy No.	Composition %			Thermal analysis (readings in degrees C)	
	Si	Mg	Fe		
117	9.53	1.81		767/699/(684)	E_3
118	9.70	.29	0.03	811/(796)/759/(709)	T_3
119	9.73	.48		809/(782)/699	
120	10.70	.76		805/(720)/**714**	
121	10.5	.71	.28	809/(729)/**714**	
122	11.03	.47	.13	**851**/(737)/716 sol./(618)	
123	11.50	.92	.08	813/722/(661)	
124	12.6	.61	.12	822/750/(676)	
125	9.84	.74		785/(759)/(746)/**699**	E_3
130	0.5	2.52	.17		
131	4.47	.06	.07	910/726	
132	4.92	.39			
133	5.38	.08	.07		
134	5.33	.80		860/**720**/(705)	
135	5.66	.86		839/(696)	
136	5.48	.96	.07	833/(726)/718/706	T_5
137	6.1	.49	.14	846/(757)/**705**/(609)	
138	6.45	.24	.37		
139	7.1	.09	.44	842/714/**701**	
140	10.70	.79	.05	785/710/705	
141	7.76	.00	.20	763/714/699	
142	7.83	.99	.02	722/710/**699**	
143	8.02	.96		729/**697**	
144	8.6	.14	.21	762/701/(678)	E_3
145	8.75	.41		750/**703**/(684)	
146	8.81	.81		751/(727)/701 sol./(676)	E_3
147	9.18	.18	.02	748/(744)/**701**/678	T_4
148	9.15	.62	.02	739/**699**/(678)	
149	9.28	.37	.02	746—742/705	(T_4)
150	9.55	.37		756/**745**/705	T_4
151	9.74	.06	.09	768/702/(692)	
152	9.98	.80	.04	756/**707**	
154	10.9	.90		789/718/(705)	
155	10.50	.08	.04	793/699	
156	11.8	.22	.13	789/739/716 sol./632	(E_2)
160	6.63	3.70		761/(720)/707—703 sol.	
161	7.0	.28	.17	740/**702**	
162	7.1	.82	.14		
163	7.7	.98	.21	704/701/**697** sol.	
164	8.28	.50	.02	718/**711**	
165	8.6	.5	.1	716/707	
166	9.10	.07		741/707/(703)	
167	9.16	.38	.03	716/**697**	E_3
168	9.76	.22		746/**720**	
169	9.83	.98	.02	731/**716**	
170	10.7	.65	.55	764/716/(633)	
171	10.69	.8		748/720/(667)	
172	13.4	.4	.03	769/**744**	
173	7.63	.91	.14	**693** sol.	E_4
176	1.97	4.86	.09	862/744	
177	6.38	.16	.15	764/716/**707**	T_5
178	8.46	.22	.03	716/701/**695** sol.	E_4
179	8.84	.29	.04	710/**701**/(699)	E_3
180	6.5	.94		756/718/**701**	T_5

Appendix A (cont.)

Alloy No.	Composition %			Thermal analysis (readings in degrees C)	
	Si	Mg	Fe		
181	10.20	4.84	0.09	733/727/**718**/(655)	
182	8.7	.72	.15	737/**709**/(674)	
183	13.95	.15	.31	744/**739**	E_1
184	8.10	.55	.13	710/(703)/**692**	E_4
186	4.36	5.0		794/**735**	
187	13.31	.99	.22	775/**759**	
188	8.25	.26	.03	766/**706**	
189	12.63	.26	.19	**763**/(721)	
190	10.4	.4	.15	755/**726**	
191	11.5	.82	.24	769/723	E_2
193	9.4	6.77	.20	762/**717**	
194	10.2	.80		729/**722**	
196	6.6	7.23	.24	824/720/(708)	T_5
197	8.80	.96	.03	829/**705**	
198	10.70	.07	.30	**723** sol.	E_2
199	1.77	.89			
200	3.59	.86			
201	4.54	.57		817/**741**	
203	0.15	8.90			
204	0.77	.08			
205	2.79	.01			
207	12.3	9.72	.21	830/818/726	
208	10.5	.83	.32		
209	10.5	.55	.35	856/762/726	
210	14.27	.90	.07		
211	14.73	9.63			
212	13.6	10.00	.03		
213	15.4	9.95	.07		
214	17.07	9.93	.05		
215	14.67	9.69	.09		
216	14.65	9.78	.13		
218	3.94	10.33	.14	858/**752**	
219	5.97	10.3	.28	880/732	
220	7.1	10.7	.14	893/714/(704)	
221	7.57	11.7	.28		
222	9.5	11.4	.56		
223	12.6	11.5	.46	863/**822**/721	E_2
224	16.1	10.8	.28	**818**/787/731	E_5
225	15.85	10.85	.27		
226	14.43	10.5	.27		
227	15.4	10.8	.25		
228	16.1	10.21	.11		
229	16.2	10.18	.06		
230	15.82	10.51	.09		
231	9.5	11.8	.28	902/725	E_2
232	7.75	.5	.33		
233	13.7	.3	.31	842/**824**	
234	13.19	.5			
235	11.43	.63			
236	15.9	.5	.14		

Appendix A (cont.)

Alloy No.	Composition %			Thermal analysis (readings in degrees C)	
	Si	Mg	Fe		
237	15.05	11.2	0.10		
238	13.3	.31	.10	855/**825**/(720)	
239	14.56	.75	.08		
240	14.36	.76	.07		
241	11.6	12.86	.21	891/**815**/765/(721)	
242	14.4	.7	.25		
243	8.2	14.1	.08	932/(716)/(708)	
244	6.2	13.1	.10		
245	9.35	.1	.12	923/(759)/722	E_2
246	9.22	.2			
247	12.4	14.9	.32	900/826	P_2
248	9.6	.0	.14	918/725	
249	8.58	.5			
250	25.86	.12	.03		
251	2.86	15.7	.22	904/(754)/(736)	
252	5.4	.9	.32	929/750	
253	0.25	.5			
254	1.58	.6			
255	6.26	.8			
256	4.35	.97			
257	10.5	16.8	.16	935/**929**/823	P_1
258	3.14	.5			
259	7.02	.20		**934**/746/701	
260	10.6	.55	.10		
261	.42	.9	.10		
262	7.8	17.1	.09	**941**/—	
263	7.1	.1	.13	**938**/(761)	
264	10.2	18.9	.19	935/930	P_1
265	11.4	.3	.28	**928**/—	
266	8.95	19.2	.25	**939**/—	
267	11.32	27.90	.59		
268	9.45	28.4	.27		
269	25.15	23.12	.07		
270	18.85	27.88	.13		
271	14.71	34.72	.05		

( ) faint thermal arrest

000 very distinct thermal arrest

Appendix B

Phase identification with X-rays.

Alloy	Chill-cast	450°	500—600°	600—700°	700—750°	750—800°	800°—	Remarks
9	α							
10	α							
23		α						
28		α						
34		α						
36		$\alpha+\gamma$			$\varkappa+\alpha+\gamma$ 710°		$\alpha+\varkappa$ 830°	
38		$\alpha+\gamma$						
39					$\varkappa+\alpha+(\gamma)$ 710°	$\varkappa+\alpha+\delta$ 790°	$\varkappa+\alpha+\delta$ 810°	
40	$\gamma+\varkappa$						$\varkappa+(\delta)$ 805°	
41					$\gamma+(\varkappa)$ 730°	$\varkappa+\delta$ 790°	$\varkappa+\delta+\gamma$ 830°	*)
43					$\gamma+\varkappa$ 710°			
44		$\gamma+\alpha$						
45	$\gamma+\varkappa$	γ					$\gamma+(\delta)$ 830°	Quenched in liquid air
46						$\varkappa+\gamma$ 790°		
48					$\gamma+\varkappa$ 730°	$\varkappa+\delta$ 790°	$\varkappa+\delta$ 815°	**)
49					$\gamma+\varkappa$ 750°		$\varkappa+\delta$ 800°	**)
50						$\gamma+\varkappa+(\delta)$ 790°		
53					$\varepsilon+\gamma$ 710°	$\gamma+(\delta)$ 750°		
57						$\varepsilon+\gamma$ 770°	$\varepsilon+\gamma$ 800°	$\delta+\varkappa$ 805° **)
58	$\gamma+\varepsilon+\delta$							
59	$\gamma+\delta+\varepsilon$				$\gamma+\varepsilon$ 750°			
62					$\gamma+\varepsilon$ 750°		$\varkappa+\delta$ 810°	**)
63	$\gamma+\delta$				γ 730°	$\gamma+\delta$ 790°		
64		$\gamma+\varepsilon$					δ 810°	
65						$\varepsilon+\gamma$ 770°		
67	$\gamma+\delta$							
69	$\varepsilon+\gamma+\varrho$				$\varepsilon+\gamma+(\eta)$ 750°			
70	$\gamma+\varepsilon+\varrho$				$\varepsilon+\gamma$ 710°	$\gamma+\varepsilon+(\eta)$ 750°		
71	$\gamma+\delta$	$\gamma+\varepsilon$						
72						$\varepsilon+\delta+(\eta)$ 790°	$\delta+\varepsilon$ 815°	***)
73	$\gamma+\delta$						$\delta+\eta+(\gamma)$ 810°	
74	$\gamma+\eta+\delta$	ε			$\varepsilon+\gamma$ 700°	$\delta+(\varepsilon)$ 770°	δ 815°	
75	$\eta+\delta+\varrho$						$\delta+\eta$ 815°	
76						ε 770°	$\delta+\eta+\varrho$ 830°	§)
77	$\eta+\varrho+(\delta)$	ε						
79	η							
80	η							
81	η	η	η	η				
82	γ						$\varkappa+\delta+(\gamma)$ 815°	§§)
86	$\alpha+(\varrho)$							
88		α						
89		$\alpha+(\varrho)$						
90		α						
91		α						
96		$\alpha+\gamma$					$\varkappa+(\alpha)$ 810°	
98	$\gamma+\varkappa+\alpha$	$\gamma+\alpha$					$\varkappa+\alpha$ 826°	
103		γ			γ 710°			
105	$\gamma+\varrho+\varepsilon+\eta$				γ 710°	γ 750°		
108		$\gamma+\varrho+(\varepsilon)$						
111		$\gamma+\varepsilon$				$\gamma+\varepsilon$ 770° $\gamma+\delta+(\varepsilon)$ 790°		

*) $\varkappa+\delta+\gamma$ corresponds to $\beta+$ liq.
**) corresponds to $\beta+\delta$ or $\delta+\beta$
***) corresponds to $\delta+$ liq.
§) corresponds to $\delta+\eta+$ liq.
§§) corresponds to $\beta+\delta+$ liq.

Appendix B (cont.)

Alloy	Chill-cast	450°	500—600°	600—700°	700—750°	750—800°	800°—	Remarks
112	$\varepsilon+\gamma$	$\varepsilon+\gamma$			ε 750°			
118	$\gamma+\varrho+(\eta)$							
120		ε						
121	$\eta+\varrho$	ε						
122		ε						
123	$\eta+\varrho+\sigma$	$\varepsilon+\sigma+(\varrho)$						
124		$\eta+\sigma$						
130		α						
131		$\alpha+(\varrho)$						
135	$\varkappa+\gamma+\alpha$	$\alpha+\gamma+(\varrho)$						
137		$\alpha+\gamma$		$\varkappa+(\alpha+\gamma)$ 609		$\varkappa+(\alpha)$ 790°		
138		$\gamma+\alpha+(\varrho)$	$\alpha+\gamma$ 570°	$\alpha+\gamma+\varkappa$ 620°				
139		$\gamma+\alpha$		$\alpha+\gamma+\varkappa$ 612°		$\varkappa+\alpha+\delta$ 790°		
141	γ	γ						
144		γ						
151	$\gamma+\varrho+(\eta)$	$\varepsilon+\gamma+(\varrho)$						
154		$\varepsilon+\varrho$						
156		$\varepsilon+\eta+\sigma$						
161		$\gamma+(\varrho)$						
162		$\gamma+\alpha+\varrho$						
163			$\gamma+\varrho$ 600°					
165		$\gamma+\varrho$						
166		$\varepsilon+\gamma+\varrho$						
167	$\varepsilon+\varrho+(\eta)$							
169		$\varepsilon+\varrho$						
170	$\eta+\varrho$	$\varepsilon+\varrho$		$\varepsilon+\varrho$ 640°				
176		$\alpha+\varrho$						
178	$\varepsilon+\varrho+(\gamma)$							
179	$\gamma+\varepsilon+\varrho+(\eta)$							
180	$\gamma+\varkappa+\alpha$	$\alpha+\gamma+\varrho$						
181	$\eta+\varrho$	$\varepsilon+\varrho$		$\varepsilon+\varrho$ 675°				
183		$\eta+\sigma$						
186		$\alpha+\varrho+(\gamma)$						
187	$\sigma+\eta$	$\sigma+\eta$						
188		$\gamma+\varrho$						
189	$\eta+\sigma$	$\varepsilon+\sigma+(\eta)$						
190				$\varepsilon+\varrho$ 670°				
191			$\varrho+\sigma+\varepsilon$ 600°					
193				$\gamma+\varrho+\varepsilon$ 630°				
194		$\varepsilon+\varrho$						
196		$\alpha+\eta+\sigma$						
198	$\varrho+\eta+\sigma$	$\varepsilon+\varrho+(\sigma)$						
199		$\varrho+\alpha$						
200		$\varrho+\alpha$						
201		$\varrho+\alpha$						
203		$\varrho+\alpha$						
204		$\varrho+\alpha$						
205		$\varrho+\alpha$						
207		$\sigma+\varepsilon+\sigma$						
208		$\varrho+\varepsilon$						
209		$\varrho+\varepsilon+\sigma$						
218		$\varrho+\alpha$						
219		$\varrho+\alpha+(\gamma)$						
220		$\varrho+(\alpha)+(\gamma)$						
221		$\varrho+\gamma$						
222		$\varrho+\varepsilon$						

Appendix B (cont.)

Alloy	Chill-cast	450°	500—600°	600—700°	700—750°	750—800°	800°—	Remarks
223	$\sigma+\varrho$	$\sigma+\varrho+\varepsilon$						
231		$\varrho+\varepsilon$						
232		$\varrho+\gamma'$						
233		σ						
243		ϱ						
244		$\varrho+\alpha$						
247		$\sigma+(\tau')$						
248		$\varrho+(\sigma)$						
249	$\varrho+\eta+(\sigma)$	$\varrho+\varepsilon+(\sigma)$						
250		$\sigma+\tau'$						
251		$\varrho+(\alpha)$						
252		$\varrho+(\alpha)$						
253		$\varrho+(\alpha)$						
254		$\varrho+(\alpha)$						
255		$\varrho+(\alpha)$						
256		$\varrho+(\alpha)$						
257		τ'						
258		$\varrho+(\alpha)$						
259		ϱ						
262		ϱ						
264	τ'							
269		$\tau'+\lambda$						
270		$\tau'+\lambda$						
271		$\tau'+\lambda+v$						

( ) faint diffraction lines

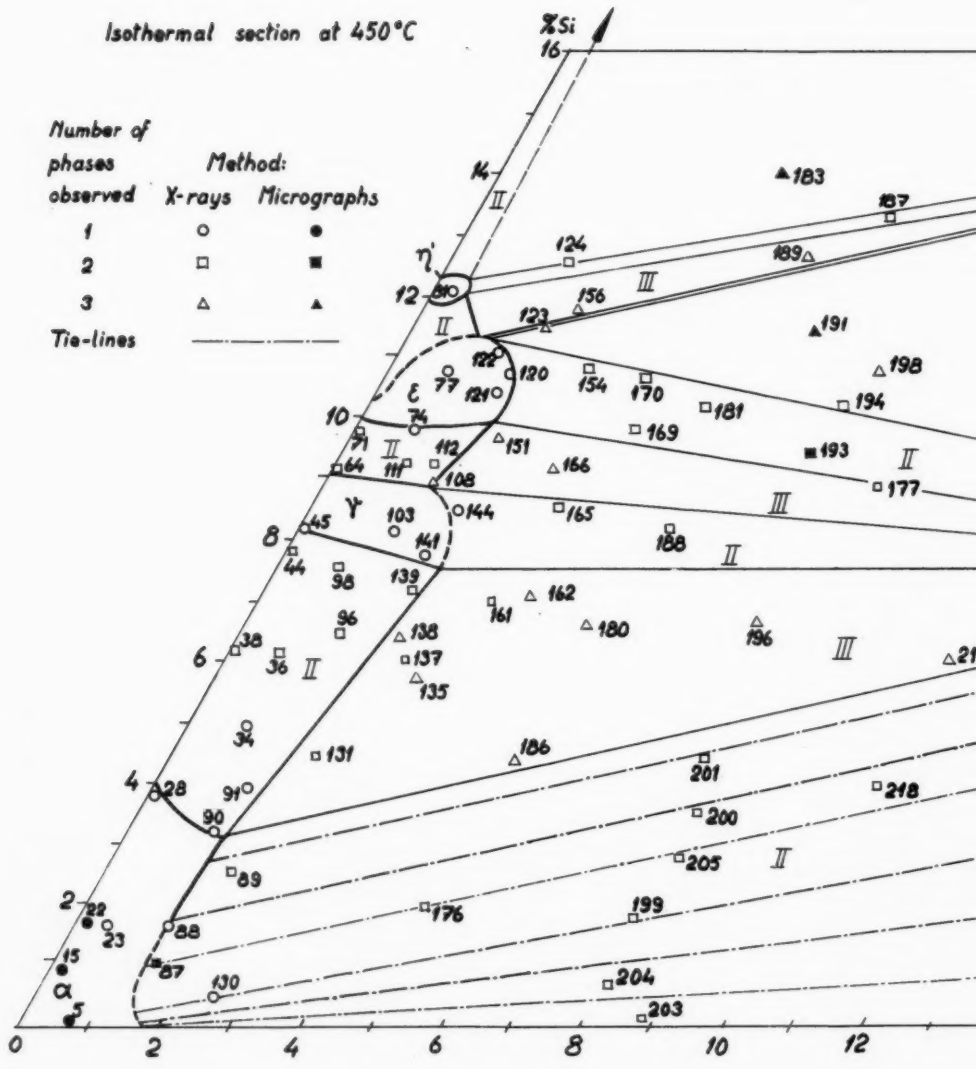

Fig. 10. The ternary diagram Cu-Mg-Si: isothermal section of the e

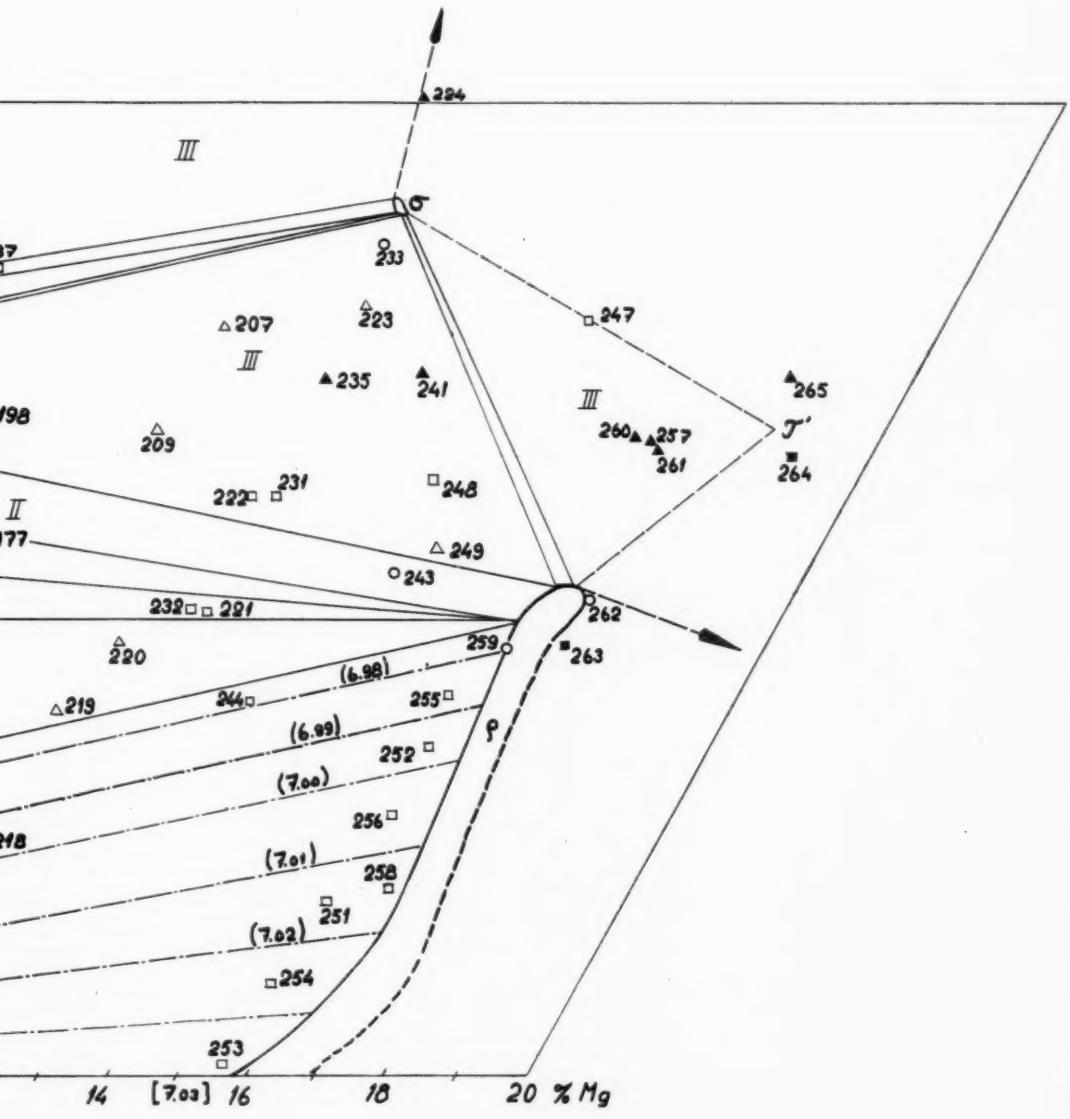

of the copper corner at 450° C.

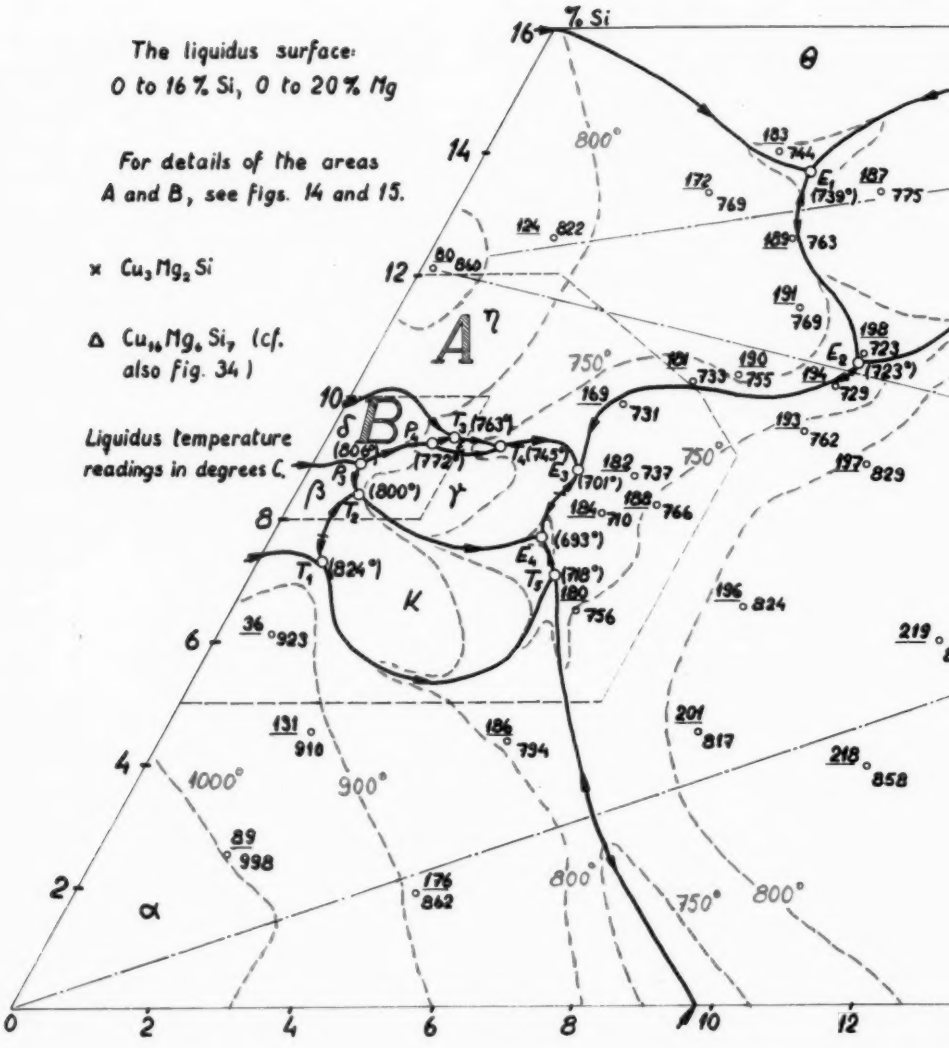

Fig. 11. The liquidus surface in the copper corner.

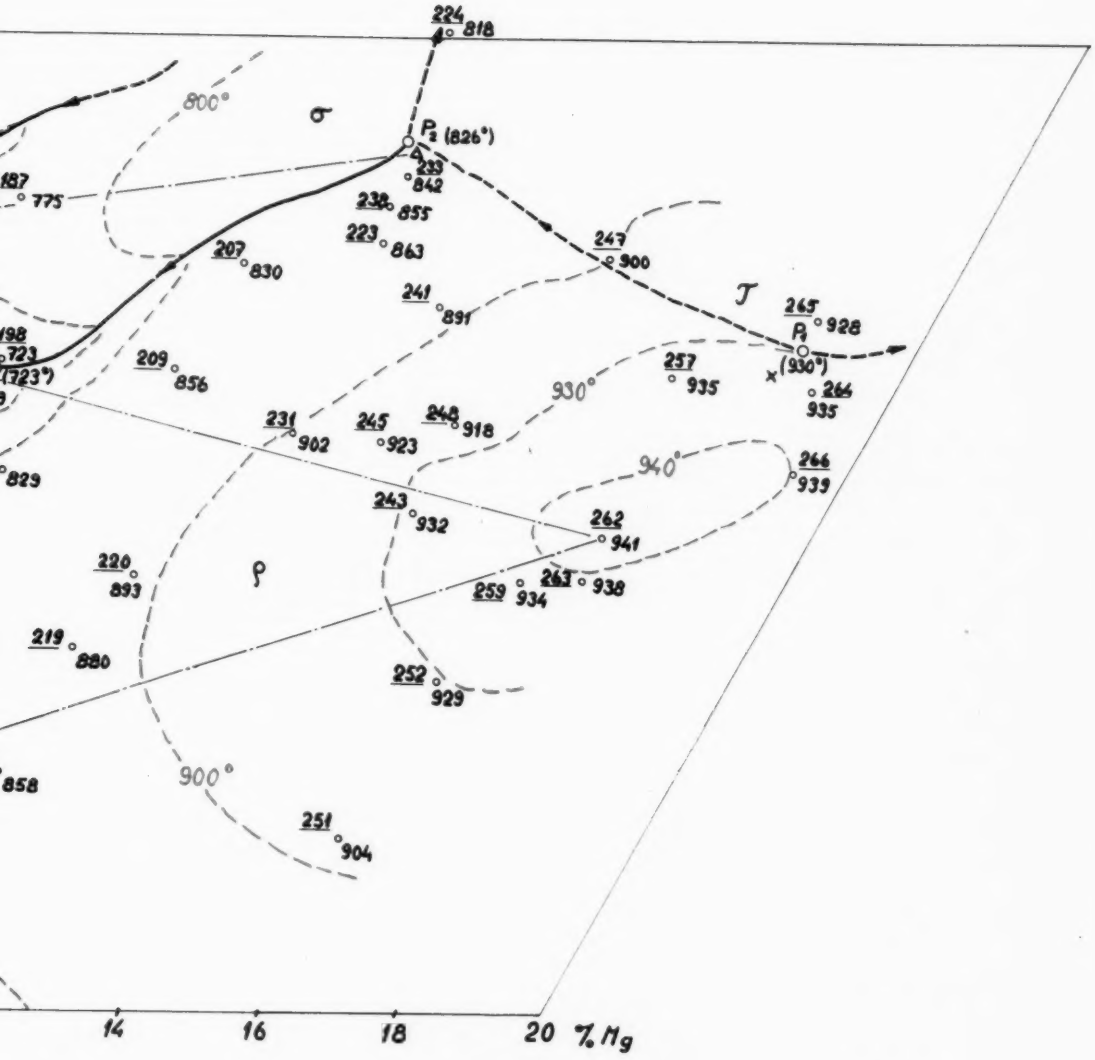
224
818
800°
σ
P₂ (826°)
233
842
238
855
223
863
207
830
247
900
241
891
τ
265
928
P₁
(930°)
209
856
257
935
264
935
930°
231
902
245
923
248
918
940°
266
939
243
932
262
941
220
893
ρ
259
934
263
938
219
880
252
929
900°
251
904
14
16
18
20 % Mg

r corner.

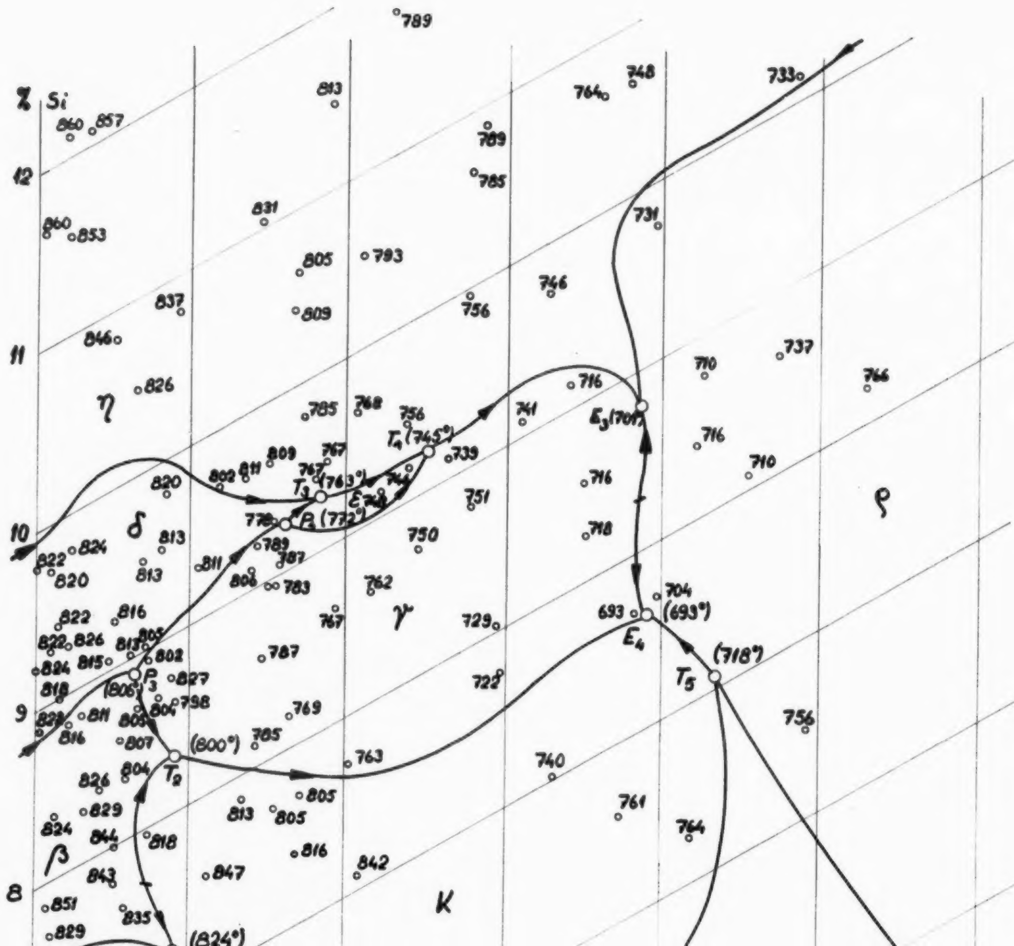
% Si
12
11
10
9
8
η
δ
β
γ
κ
ρ
T_2 (800°)
T_3 (763°)
T_4 (745°)
T_5 (718°)
P_3 (806°)
P_4 (772°)
E_3 (701°)
E_4 (693°)
(824°)

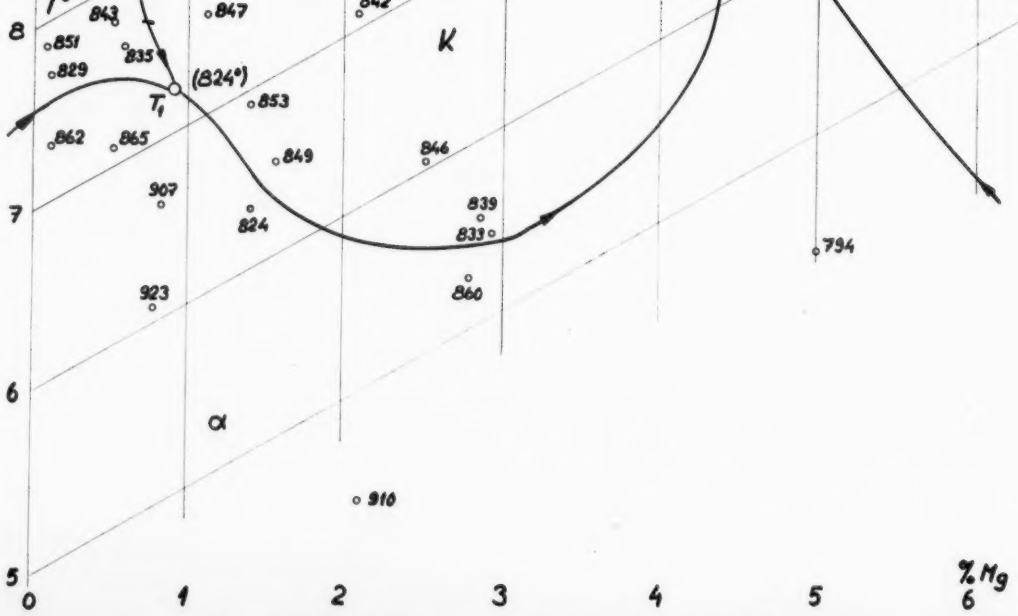

Fig. 14. Detail of fig. 11: part A (5 to 12 % Si, 0 to 5 % Mg).

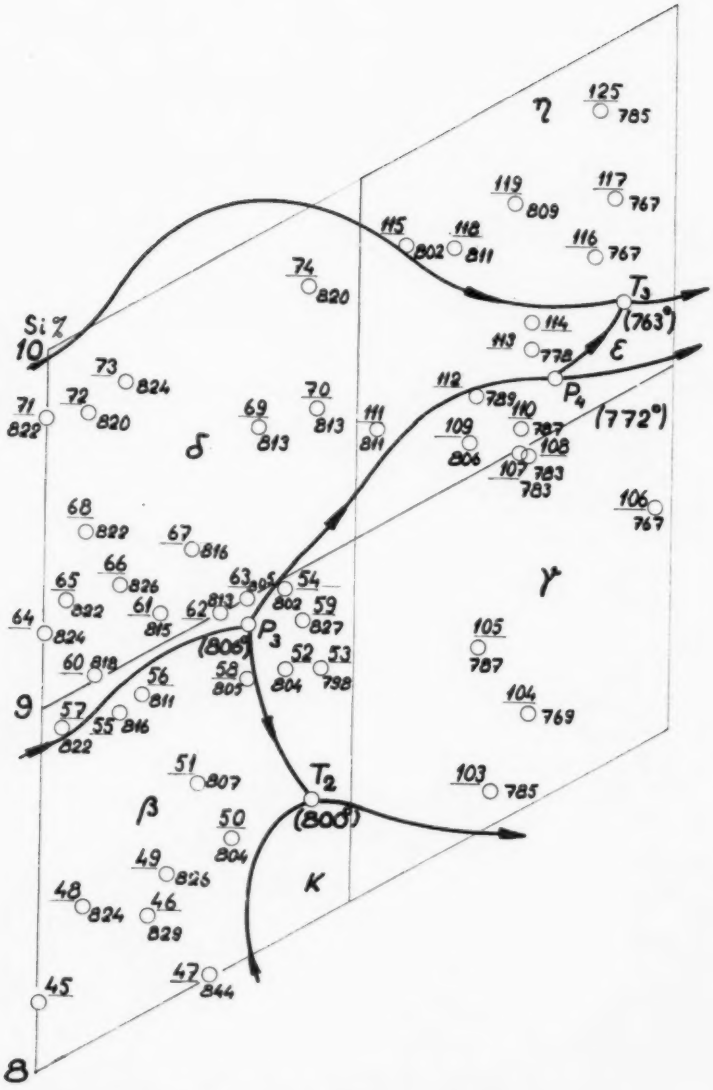

Fig. 15. Detail of fig. 11: part B (8 to 10 % Si, 0 to 2 % Mg).

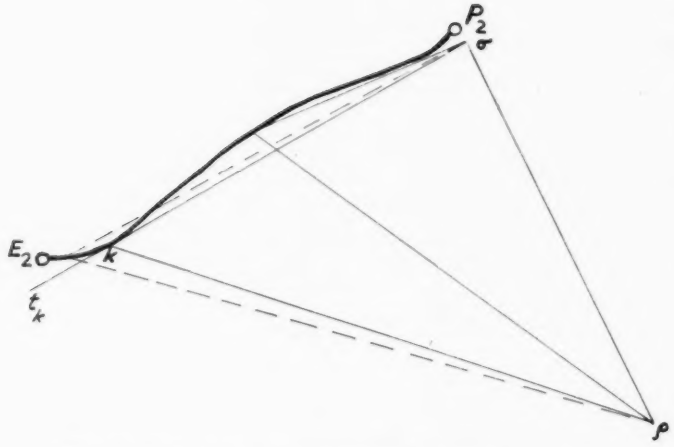

Fig. 18. Line of twofold ϱ—σ-saturation, with inflexion point.

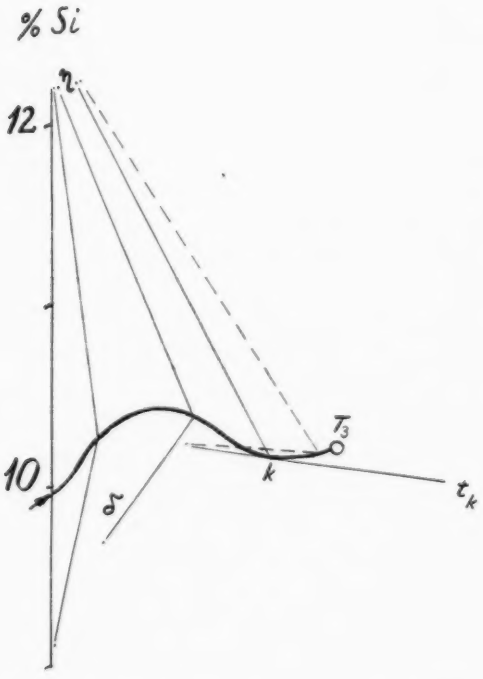

Fig. 19. Line of twofold δ—η-saturation, with inflexion point.

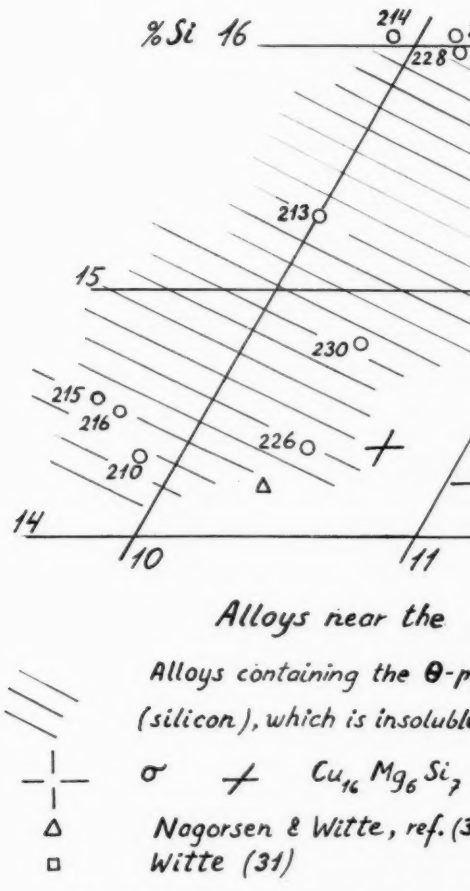

Fig. 34. θ-content in alloys near the theor

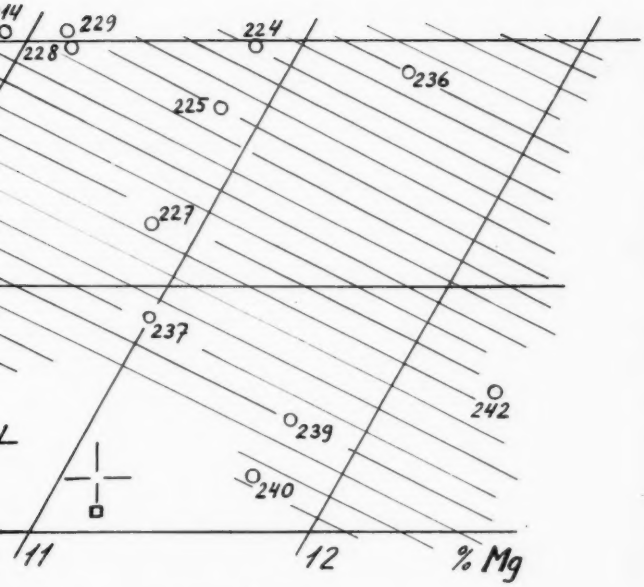

the σ - composition.

he θ-phase,

nsoluble in $HCl + HNO_3$.

$Mg_6 Si_7$

, ref. (32)

the theoretical σ-composition. (Shaded area = precipitation of θ).

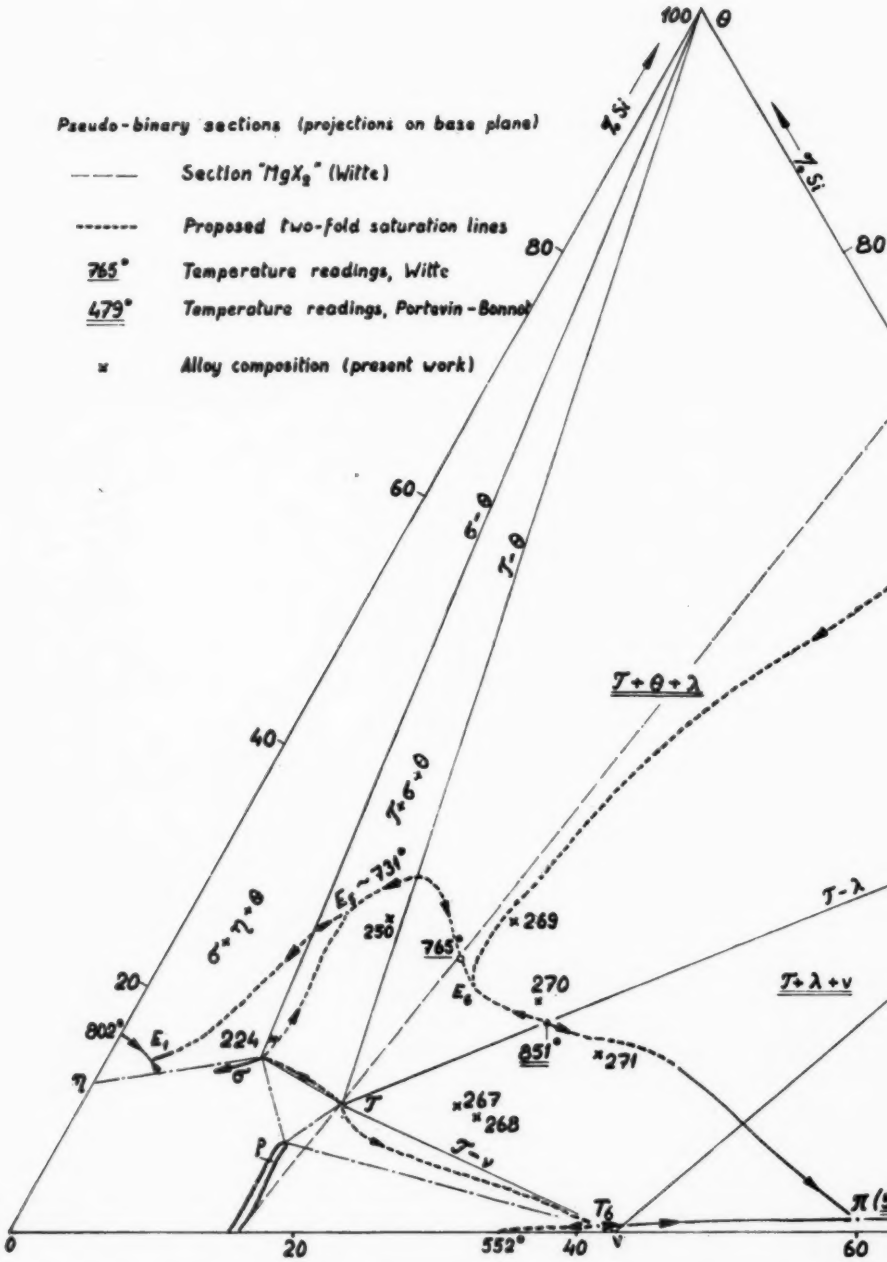

Fig. 40. Pseudo-binary sections and some lines of twofold saturation in the sy

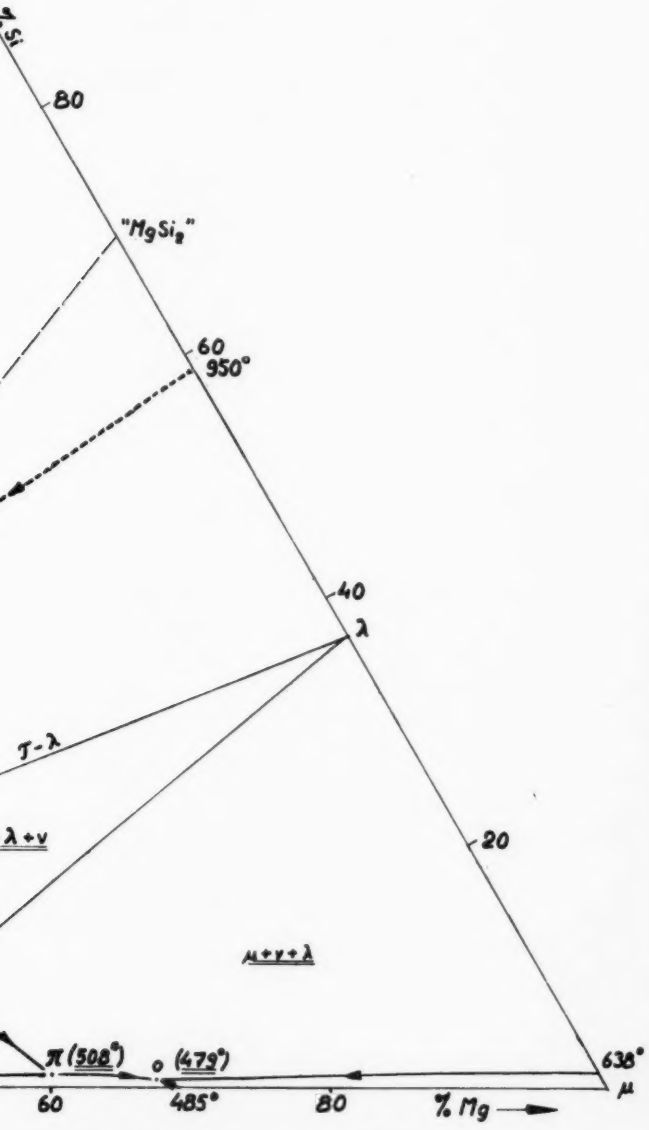

n the system Cu-Mg-Si (projection on base plane).

Appendix C

Diagram of X-ray powder diffraction p

APPENDIX C : X - RAY POWDER PATTERNS.

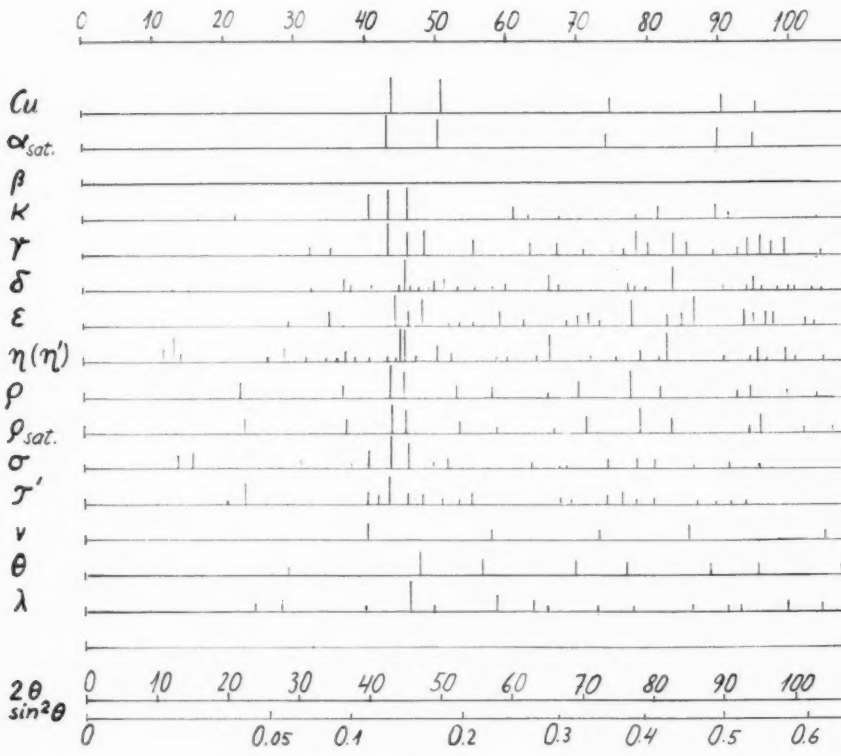

fraction patterns.

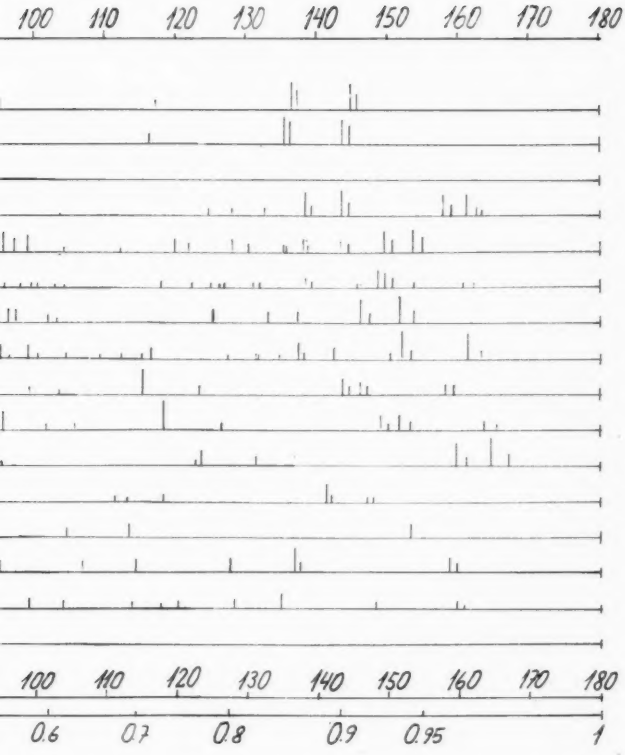

THE LAST VOLUMES OF ACTA POLYTECHNICA

Chemistry including Metallurgy Series

(The predecessor of Acta Polytechnica Scandinavica)

Volume 4

Nr 1 SJÖSTRÖM, E: *Über die Verwendung von Ionenaustauschern für die Sorption und Trennung von Ketonen.* Acta P 144 (1954), 50 pp, Sw. Kr 8: 00 UDC 661.183.12:66.067.75:547.284

Nr 2 LEDEN, I and SCHÖÖN, N-H: *The Solubility of Silver Azide and the Formation of Complexes between Silver and Azide Ions.* Acta P 155 (1954), 17 pp, Sw. Kr 4: 00 UDC 662.413.1

Nr 3 SANDFORD, F, and FRANSSON, S: *The Refractoriness of Some Types of Quartz and Quartzite.* I. Acta P 156 (1954), 27 pp, Sw. Kr 6: 00 UDC 666.346.6:666.361.2

Nr 4 SÖNNERSKOG, S: *Some Ethers of Cellulose and Starch.* Acta P 157 (1954), 72 pp, Sw. Kr 10: 00 UDC 661.892

Nr 5 HEDVALL, J A: *Reactions with Activated Solids.* Acta P 163 (1954), 23 pp, Sw. Kr 5: 00 UDC 541.124-188:548.4

Nr 6 SVENSSON, J: *A New Formula for Particle Size Distribution of Products Produced by Comminution.* Acta P 167 (1955), 53 pp, Sw. Kr 6: 00 UDC 539.215:621.926

Nr 7 HEDVALL, J A, NORDENGREN, S und LILJEGREN, B: *Über die Thermische Zersetzung von Kalziumsulfat bei Niedrigen Temperaturen.* Acta P 170 (1955), 18 pp, Sw. Kr 5: 00 UDC 661.842.532:66.092.4

Nr 8 DAHLGREN, S-E: *On the Break-down of Thixotropic Materials.* Acta P 171 (1955), 18 pp, Sw. Kr 3: 50 UDC 541.182.025

Nr 9 SANDFORD, F, and FRANSSON, S: *The Refractoriness of Some Types of Quartz and Quartzite.* II. Acta P 173 (1955), 24 pp, Sw. Kr 5: 00 UDC 666.76:549.514.51

Nr 10 BJÖRKMAN, L, BJÖRKMAN, M, BRESKY, A, ENEBO, L, and RENNERFELT, J: *Experiments on the Culture of Chlorella for Food Purposes.* Acta P 176 (1955), 18 pp, Sw. Kr 4: 00 UDC 663.11:582.2

Nr 11 WRANGLÉN, G: *Dendrites and Growth Layers in the Electrocrystallization of Metals.* Acta P 182 (1955), 42 pp, Sw. Kr 6: 50 UDC 669.017:548.232.4:669.017:548.52

Nr 12 MATTSSON, E: *The Electrode Process in Metal Deposition from Aqueous Solutions.* Acta P 184 (1955), 56 pp, Sw. Kr 6: 50 UDC 541.135:621.357

Nr 13 EDHBORG, A: *Studies on a Water-Soluble Material from the Masonite Process.* Acta P 197 (1956), 87 pp, Sw. Kr 12: 50 UDC 547.454:542.938:542.941
out of print

ACTA POLYTECHNICA SCANDINAVICA

Chemistry including Metallurgy Series

Ch 1 JART, A: *Fat Rancidity. Summaries of Papers Presented at the 2nd Scandinavian Symposium on Fat Rancidity.* (Acta P 242/1958) 72 pp, Sw. Kr 7: 00 UDC 665.112.2

Ch 2 ERÄMETSÄ, O: *Ion Characteristics; a New Way of Assessing the Chemical Properties of Ions.* (Acta P 249/1958) 22 pp, Sw. Kr 7: 00 UDC 541.7

Ch 3 ERÄMETSÄ, O: *On the Decomposition of Potash Felspar.* (Acta P 260/1959) 17 pp, Sw. Kr 7: 00 UDC 553.61:542.92

Ch 4 *Report of the Committee on Slaughtering Methods Appointed by the Danish Academy of Technical Sciences at the Request of the Ministry of Justice.* (Acta P 264/1959) 35 pp, Sw. Kr 7: 00 UDC 637.513.22

Ch 5 MÄKIPIRTTI, S: *On the Sintering of W-Ni-Cu Heavy Metal.* (Acta P 265/1959) 69 pp, Sw. Kr 7: 00 UDC 621.762:669.275.24.3

Ch 6 PAULSEN, A: *Constitution des Quatre Isomeres de Position des Chloro et Aminomethylbenzodioxannes-1,4, Substitues dans le Noyau Benzenique.* (Acta P 270/1960) 94 pp, Sw. Kr 7: 00 UDC 547.84:615.45

Ch 7 DAHLGREN, S-E: *Physico-Chemical Background of Phosphoric Acid Manufacture by Wet Processes.* (Acta P 271/1960) 15 pp, Sw. Kr 7: 00 UDC 661.634

Ch 8 SUNDIUS, N: *Felspar and its Influence on the Reactions in Ceramics during Burning.* (Acta P. 272/1960), 29 pp, Sw. Kr. 7: 00 UDC 666.6.041.9:553.61

Ch 9 DAHL, OLE: *Gamma Irradiation of Vacuum-Packed Sliced Meat Products.* (Acta P. 276/1960), 24 pp, Sw. Kr. 7: 00 UDC 664.91.037:539.166

Ch 10 ENEBO, LENNART AND PEHRSON, STIG O: *Thermophilic Digestion of a Mixture of Domestic Sewage Sludge and Cellulose Materials.* (Acta P. 281/1960) 40 pp, Sw. Kr. 7: 00 UDC 663.1:628.35:676.16

Ch 11 ASCHAN, L. J.: *Studies on the ternary system Cu-Mg-Si.* (Acta P. 285/1960) 46 pp, Sw. Kr. 7: 00 UDC 669.018.669.3.721.782 (084.2)

Price Sw. Kr. 7.00